

ACCELERATED PHOSPHORUS MAGNETIC RESONANCE SPECTROSCOPIC
IMAGING USING COMPRESSED SENSING METHOD

by

Nurten Ceren AŞKIN

Submitted to the Institute of Graduate Studies in
Science and Engineering in partial fulfillment of
the requirements for the degree of

Master of Science

in

Biotechnology

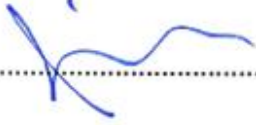
Yeditepe University

2013

ACCELERATED PHOSPHORUS MAGNETIC RESONANCE SPECTROSCOPIC
IMAGING USING COMPRESSED SENSING METHOD

APPROVED BY:

Asst. Prof. Dr. Esin ÖZTÜRK IŞIK
(Supervisor)



Prof. Dr. Mustafa ÇULHA



Assoc. Prof. Dr. Haluk KÜÇÜK



DATE OF APPROVAL:/...../.....

ACKNOWLEDGEMENTS

I am heartily thankful to my professor, Asst. Prof. Dr. Esin Öztürk Işık, whose encouragement, guidance and support from the initial to the final level enabled me to develop an understanding of the subject. I would like to extend my gratitude to Prof. Dr. Mustafa Çulha and Assoc. Prof. Dr. Haluk Küçük, for teaching me useful knowledge during my education years.

Lastly, I would like to thank to Yeditepe University Hospital to let me use their MRI scanner in this project. I am very thankful to other assistants in our laboratory, Hale Hatay, Çağıl Gümüş and Füsun Er for their support.

Nurten Ceren AŞKIN

ABSTRACT

ACCELERATED PHOSPHORUS MAGNETIC RESONANCE SPECTROSCOPIC IMAGING USING COMPRESSED SENSING METHOD

The purpose of this simulation study is to assess the performance of accelerated phosphorus magnetic resonance spectroscopic imaging (^{31}P MRSI) using latest fast MR imaging technique, called compressed sensing. A volunteer was scanned at a 3T MR scanner (Philips Medical Systems, Best, Netherlands) using a ^{31}P surface coil. Acquired ^{31}P spectra dataset was quantified using AMARES tool in jMRUI. Healthy and tumor datasets were created in MATLAB (The Mathworks Inc., Natick, MA, USA) based on metabolite peak intensities and ratios of ^{31}P spectra dataset. A 2D 32x32 sized phosphorus spectra dataset which contains healthy and tumor (10x10 voxels on the left top side) regions were simulated. A randomly undersampled pattern which reduces k-space data along x by a reduction factor of 2.23 was implemented to k-space of 2D phosphorus spectra dataset. This undersampled k-space was inverse Fourier transformed along k_y and then k_x -f data was reconstructed for each y point using Sparse MRI software package that uses compressed sensing (CS) method. Results of our simulation study showed that compressed sensing applied datasets had higher signal to noise (SNR) ratio than the original datasets due to denoising effects of compressed sensing reconstruction technique. However, peak ratios were similar between both compressed sensing and original datasets. This study indicated that compressed sensing reconstruction could be used for faster phosphorus magnetic resonance spectroscopic imaging.

ÖZET

SIKIŞTIRILMIŞ ALGILAMA METODU KULLANILARAK HIZLI FOSFOR MANYETİK REZONANS SPEKTROSKOPİK GÖRÜNTÜLEME

Bu simülasyon çalışmasının amacı, en son çıkan hızlı MR görüntüleme tekniklerinden olan sıkıştırılmış algılama kullanılarak hızlandırılmış fosfor manyetik rezonans spektroskopik görüntülemenin (^{31}P -MRSG) performansını değerlendirmektir. Bir gönüllü 3T MR tarayıcısında (Philips Medical Systems, Best, Netherlands) ^{31}P yüzey sarmalı kullanılarak görüntülendi. Elde edilen ^{31}P spektra veri kümesi jMRUI içindeki AMARES aracıyla sayısallaştırıldı. Sağlıklı ve tümörlü veri kümeleri ^{31}P spektra veri kümelerinde metabolit pik yoğunluklarına ve oranlarına bakılarak MATLAB'da (The Mathworks Inc., Natick, MA, USA) oluşturuldu. 2 boyutlu 32×32 'lik sağlıklı ve tümörlü (10×10 voksel, üst sol köşede) bölgelerden oluşan bir fosfor veri kümesi simüle edildi. k-uzayını x boyunca 2.23 lik azalma faktörü ile düşüren bir rastgele altörneklenmiş örüntü, iki boyutlu fosfor spektra veri kümesinin k-uzayına uygulandı. Bu azaltılmış k-uzayı, k_y boyunca ters Fourier dönüştürülüp, k_x -f verisi her y noktası için sıkıştırılmış algılama (SA) metodu olan Sparse MRI yazılım paketi kullanılarak geri çatıldı. Simülasyon çalışmasının sonuçlarında sıkıştırılmış algılama uygulanmış veri kümesinin orijinal veri kümesine oranla daha yüksek sinyal gürültü oranına (SGO) sahip olduğu ve bunun da nedenin sıkıştırılmış algılama geri çatma tekniğinin gürültüsüzlük etkisinin olduğu görüldü. Ancak pik oranları, sıkıştırılmış algılama ve orijinal veri kümeleri için de benzer çıktı. Bu çalışma, sıkıştırılmış algılama geri çatmasının hızlandırılmış fosfor manyetik rezonans görüntüleme için kullanılabilir olduğunu göstermiştir.

TABLE OF CONTENTS

LIST OF FIGURES	v
LIST OF TABLES	vii
1. INTRODUCTION	1
2. BACKGROUND	3
2.1 MAGNETIC RESONANCE IMAGING	3
2.2 MAGNETIC RESONANCE SPECTROSCOPIC IMAGING	5
2.3 ³¹ P PHOSPHORUS MAGNETIC RESONANCE SPECTROSCOPIC IMAGING ..	9
2.4 IMAGE SELECTED IN VIVO SPECTROSCOPY	11
2.5 WAVELET TRANSFORM	16
2.6 COMPRESSED SENSING METHOD	17
2.7 CONJUGATE GRADIENT METHOD	18
2.8 STATISTICAL METHODS	21
2.8.1 Bland Altman Method	21
2.8.2 Wilcoxon Signed Rank Sum Test	21
3. MATERIAL AND METHODS	24
3.1 DATA ACQUISITION	24
3.2 DATA PROCESSING	24
3.3 SPARSE MRI	26
3.4 DATA ANALYSIS	26
4. RESULTS	28
5. DISCUSSION	36
6. REFERENCES	37
APPENDIX A	40
APPENDIX B	41
APPENDIX C	44
APPENDIX D	45

LIST OF FIGURES

Figure 2.1	High resolution anatomical images of a human brain. The images from left to right represent sagittal, coronal and axial views of the brain , respectively	4
Figure 2.2	Spin echo imaging.....	5
Figure 2.3	MR spectrum of signal amplitude versus frequency (frequency increases towards left)	6
Figure 2.4	Sample spectra of ^{13}C MRSI (top left), ^1H MRSI (top right) and ^{31}P MRSI (bottom)	8
Figure 2.5	^{31}P MRSI spectra from a healthy volunteer. Main ^{31}P spectrum metabolite peaks are clearly shown	11
Figure 2.6	MR anatomical images of brain tumor patients and quantification of ^{31}P MRSI data in AMARES tool within jMRUI.....	11
Figure 2.7	One dimensional ISIS with two measurements and it localizes the spectrum to a slice.....	13
Figure 2.8	Two dimensional ISIS with four measurements and it localizes the spectrum to a column	14
Figure 2.9	Three dimensional ISIS method which needs eight measurements to localize the spectrum to the voxel, S_{ABC}	15
Figure 2.10	An example of 2D Wavelet transform using Wavelet toolbox in MATLAB	16

Figure 3.1	The random undersampling pattern for one of the frequency points in k-space. In total, %56.25 of all the k-space points were set to zero (R=2.23)	25
Figure 3.2	The flowchart of ^{31}P MRSI data preparation scheme	26
Figure 4.1	Phosphorus MR spectra of six voxels for original (left) and compressed sensing (right) datasets	28
Figure 4.2	Bland Altman statistical test plot of Pi and PCr peak ratios for healthy region.....	31
Figure 4.3	Bland Altman statistical test plot of Pi and PCr peak ratios for tumor region (no outliers)	31
Figure 4.4	Bland Altman statistical test plot of PCr and β -ATP peak ratios for healthy region.....	32
Figure 4.5	Bland Altman statistical test plot of PCr and β -ATP peak ratios for tumor region (no outliers).....	32
Figure 4.6	Bland Altman statistical test plot of PCr and PE peak ratios for healthy region.....	33
Figure 4.7	Bland Altman statistical test plot of PCr and PE peak ratios for tumor (no outliers) region	33

LIST OF TABLES

Table 2.1	³¹ P MRS metabolite peak locations, and their roles in biological events.....	9
Table 4.1	Metabolite Ratios In Tumor And Healthy Regions For The Original (O) And Compressed Sensing (CS) Datasets	29
Table 4.2	Bland Altman Test Results For The Difference Of Peak Ratios In The Original And Compressed Sensing Datasets For Tumor And Healthy Regions.....	29
Table 4.3	SNR Values Of Metabolite Ratios In Tumor And Healthy Regions And Their Ratios Of The Original (O) And Compressed Sensing (CS) Datasets	34
Table 4.4	Ratio Of Tumor Over Healthy Mean Peak Heights For Each Of Metabolite Peaks In Both Datasets.....	35

1. INTRODUCTION

Magnetic resonance imaging (MRI) is the most commonly used medical imaging modality in clinic and research due to its non-invasive property. There are many advanced MR imaging techniques used in clinics. One of them is MR spectroscopic imaging (MRSI) which detects the biochemistry of the tissues of interest. Proton MR spectroscopic imaging (^1H MRSI) is the most common type of MRSI since high abundance of H content in human body. Phosphorus magnetic resonance spectroscopic imaging (^{31}P MRSI) is another type of MRSI method which detects the phosphorus content in the body. ^{31}P MRSI can provide important information regarding the energetic and ischemic status including membrane synthesis and degradation, and pH of tissue. ^{31}P MRSI can detect various metabolites and the major ones are phosphocreatine (PCr), phosphorylcholine (PC), phosphorylethanolamine (PE), inorganic phosphate (Pi), glycerophosphorylcholine (GPC), γ -ATP, α -ATP, β -ATP, and glycerophosphorylethanolamine (GPE).

Previous studies showed that phosphorus metabolite levels are different between healthy brain tissue and brain tumors [1, 2]. When the brain tissue gets ischemic, ATP production comes from hydrolysis of PCr catalyzed by creatine kinase leading to a reduction of PCr/ β -ATP ratio in ^{31}P -MRSI [2], and the breakdown of glycogen to lactic acid which can be observed as the lactate peak in proton MR spectra [3]. Pi increases at ischemia state because of increased ATP hydrolysis and this is not matched by ATP synthesis which leads an increase in Pi/PCr ratio [1]. Phosphorylcholine (PC) and phosphorylethanolamine (PE) are called phosphomonoesters (PME) which are produced from choline and ethanolamine phosphorylation during membrane synthesis. During membrane degradation GPC and GPE peaks are occurred, which are called phosphodiesteres (PDE). Increase of PME and PDE peaks shows the increase of membrane synthesis and degradation separately. In ^1H MRSI these separate changes can be only seen as one choline peak. So, ^{31}P MRSI gives separate information about the activity of cell synthesis and degradation of tumor tissue. A significant reduction in the ratio of PCr/Pi and an increase of pH levels in brain tumors were reported by Hubesh et al [1]. An alkaline environment and a decrease of PCr and PDE metabolite peaks for meningiomas were observed by Maintz et al. They also

discovered a slight alkalization (pH=7.09) and more than two factor reduction in the ratio of PDE/ α -ATP peaks for low grade gliomas [2].

Although phosphorus MR spectroscopy gives quite important information about healthy tissue and brain tumors it has not been widely used in clinics. ^{31}P is 15 times less MR sensitive than ^1H . ^{31}P MRSI needs large voxels and several data acquisitions for a sufficient signal to noise ratio (SNR). As a result it has long data scan time. Several methods have been developed for acquiring faster ^{31}P MRSI data, and one of them was published by Obruchkov et al. They implemented flyback echo planar imaging (EPI) for ^{31}P MRSI [4]. But this sequence is not available in clinical settings and there might be regridding errors in reconstruction. Srinivasa-Raghavan et al. implemented generalized autocalibrating partially parallel acquisitions (GRAPPA) method for faster ^{31}P MRSI on liver [5]. Multi-channel RF coils are needed for GRAPPA method to reconstruct undersampled data. However, phosphorus sensitive multi-channel coils are not widely available in clinical settings. Another issue is SNR loss. When accelerating ^{31}P MRSI data, SNR decreases since SNR is proportional to the root of data acquisition time. So, flyback EPI and GRAPPA methods have not been widely used for fast ^{31}P MRSI.

Compressed sensing (CS) is the latest fast data acquisition method. Compressed sensing uses a different reconstruction technique, where k-space should be randomly undersampled. Compressed sensing uses a regularization algorithm and in our study conjugate gradient method was used. In previous studies, it has been proposed that compressed sensing resulted in less SNR penalty than other fast imaging methods due to its denoising effect [6]. It has been successfully applied to ^{13}C MRSI [7, 8]. In this study we explored the feasibility of compressed sensing method for accelerating ^{31}P MRSI.

2. BACKGROUND

2.1 MAGNETIC RESONANCE IMAGING

Magnetic resonance imaging (MRI) is a non invasive medical imaging method which has a wide usage all around the world. This method, unlike the usual radiographs does not use radiation. MRI is used for diagnosis and research in clinics, however, it does not have a function for treatment. There have been several research studies including MRI such as hardware and software developments, animal experiments, MR image enhancement techniques, fast MRI methods. MRI is widely used for diagnosis and localization of brain tumors in clinics.

The working principle of MRI is based on the radiowaves which are directed at protons, the nuclei of hydrogen atoms, in a strong magnetic field (1.5T, 3T, 7T etc.). The protons are first excited and then relaxed, and they emit radio signals, which are later processed in a computer to form an image. In the body, protons (H) are most abundant in water (H₂O) so that an MRI image shows differences in the water content and distribution in various body tissues. Different kinds of tissues in the same organ can easily be distinguished by MRI. For instance white and gray matter of brain, soft tissue and hard tissue are just some examples.

Typically an MRI exam consists of two to six imaging sequences, each lasting two to 15 minutes. Each sequence has its own degree of contrast and shows a cross section of the head in one of several planes (right to left, front to back, upper to lower) (Figure 2.1). MRI can obtain anatomical and functional images at the same time.

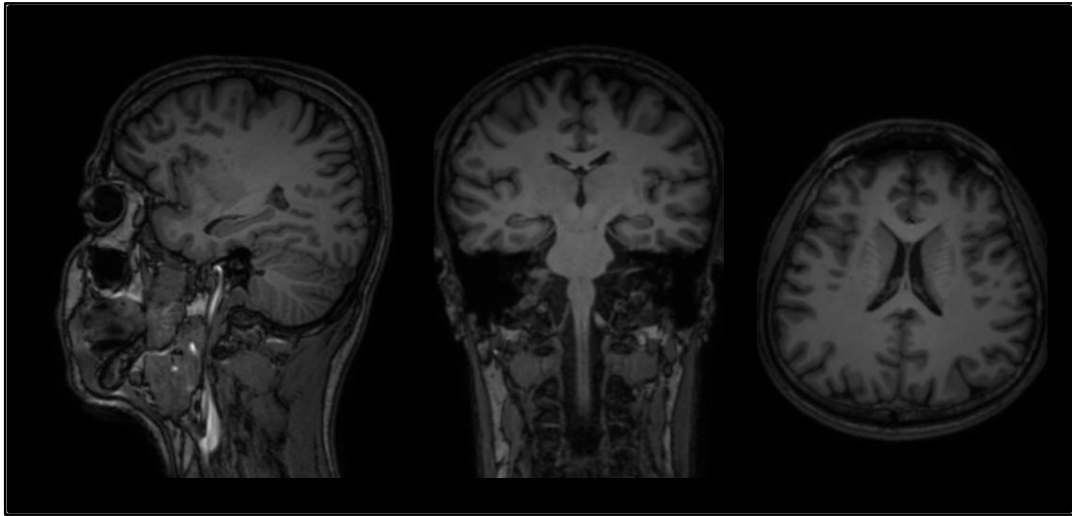


Figure 2.1 High resolution anatomical images of a human brain. The images from left to right represent sagittal, coronal and axial views of the brain, respectively

In principle, slices are created from a volume of tissue. For each image, tissues of interest are placed in the right location in the MR image. This process is called spatial localization. There are three physical gradients (X, Y, Z) in an MRI system. Gradients create changes in magnetic field strength at different locations by current in opposite sides in the coils. Change in magnetic field strength allows for spatial localization. Gradients in an MRI system can select slice, or encode frequency and phase. These gradients let the system to place every voxel of tissue into the right place in an MR image. Their function depends only on when X, Y, Z gradients are activated during the repetition time (TR) period.

The first step of acquiring an MR image is activating a slice select gradient. Here, a slice of tissue will be selected to be imaged. The type of physical gradient for this step depends on the selected planes such as axial, coronal and sagittal planes. We select a specific range of frequencies using an RF coil. By this way only the spins that are precessing within that range of frequencies will be excited. To be able to excite tissues, RF must be perpendicular to B_0 and it must be at the Larmor Frequency,

$$\omega = -\gamma B \quad (2.1)$$

where ω is the angular frequency, γ is the gyromagnetic ratio ($\gamma_{1H}=42.58$ MHz/T, $\gamma_{31P}=17.2$ MHz/T), and B is the magnitude of the magnetic field.

Gradient must be activated every time to make a slice selection. Another step of making an MR image is called 'in-plane resolution' which is a spatial localization within a slice. The tissue within the slice that we have selected must be localized in two directions. Phase encoding (PE) and frequency encoding (FE, readout) gradients are used for this purpose. Frequency encoding provides spatial localization in one direction (more FE points=better resolution). Phase encoding gradient is activated to different amplitude at each TR. When PE gradient is activated the frequencies along that axis change. More PE steps give better spatial resolution. Signals are acquired in both axes in k-space. K-space is formed through the time integral of the gradients. When the k-space is full of frequencies, Fourier transform of it is taken which gives us final 'MR image'. Figure 2.2 shows a spin echo pulse sequence with the gradients on the left, and on right k-space of it can be seen.

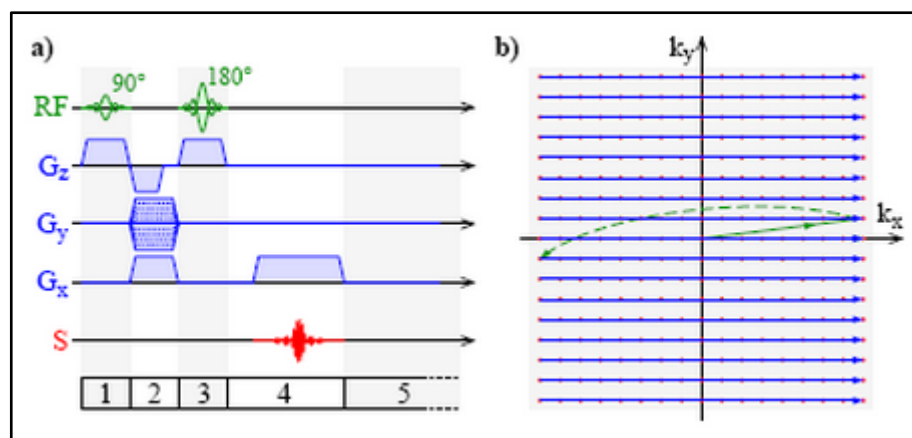


Figure 2.2 Spin echo imaging [9]

2.2 MAGNETIC RESONANCE SPECTROSCOPIC IMAGING

Magnetic resonance spectroscopic imaging (MRSI) is an advanced MRI method which provides molecular information about the tissue of interest in addition to anatomical information provided by MRI. MR spectroscopic imaging detects the concentration of important molecules, which have main roles in biologic events. Unlike conventional MRI, MRSI uses frequency to encode chemical information instead of spatial information. MRS

can be localized to a single region or via phased encoding in multiple directions through which MRSI or chemical shift imaging can be obtained. Instrumentation of MRSI is just like MRI. There are magnet, gradients, RF excitation-reception system, and working station (computer).

Nuclear magnetic resonance (NMR) was first discovered in 1946 by Felix Bloch and Edward Mills Purcell [10], [11]. They were awarded the Nobel Prize in Physics for discovering NMR separately. Firstly NMR was an experiment to determine the nuclear magnetic moments of the nuclei. Protons in different environment have different frequencies which makes it distinguishable by NMR. NMR spectrometers use a constant magnetic field strength, B_0 . Then a narrow range of frequencies is applied to obtain the resonance of all protons. Only nuclei which has odd mass numbers (^1H , ^{13}C , ^{19}F and ^{31}P) or odd atomic numbers (^2H , and ^{14}N) create NMR signals. Figure 2.3 shows an example of MR spectrum, in which frequency increases towards left.

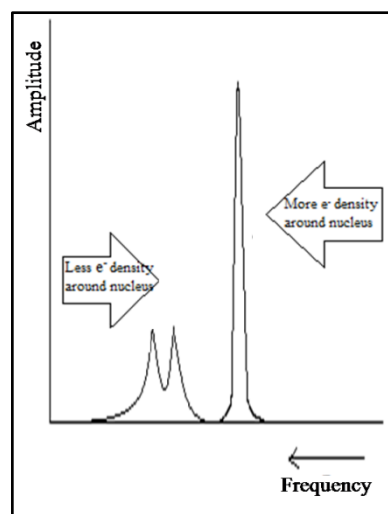


Figure 2.3 MR spectrum of signal amplitude versus frequency (frequency increases towards left)

In a magnetic field, there are two energy states for a proton. Lower energy state is in which nucleus is aligned in the same direction as B_0 . Second, higher energy state is in which nucleus is aligned against B_0 . When an external energy source ($h\nu$) that matches the energy difference (ΔE) between lower energy and higher energy states is applied, the energy is

absorbed which causes the nucleus to spin flip from one orientation to another. The energy difference between these two nuclear spin states is within the low frequency RF region of the electromagnetic spectrum. An applied magnetic field B_0 , measured in tesla (T), and the frequency ν of radiation used for resonance, measured in hertz (Hz), or megahertz (MHz) are two variables to characterize NMR. A nucleus is in resonance while it absorbs RF radiation and spin flips to higher energy state. The frequency, which is required for resonance, and applied magnetic field strength are related.

The magnitude of spin angular momentum (S) of a nuclear system can be transformed into solution of Schrödinger equation [12]:

$$S^2 = \left(\frac{h}{2\pi}\right)^2 s(s+1) \rightarrow \|s\| = \frac{h}{2\pi} \sqrt{s(s+1)} \quad (2.2)$$

where, s indicates the quantum number for the spin angular momentum, and h is Plank's constant. Since s is limited to non-negative integer and half integer values, spin angular momentum S is differentiated.

Molecular imaging methods provide better localization and characterization of brain tumors [13]. Most popular MRSI technique is proton MR spectroscopic imaging (^1H MRSI) due to its proton (H) content in water (H_2O) which is quite abundant in human body. Choline (Cho), creatin (Cr), N-acetylaspartate (NAA) are three main metabolite peaks observed in the brain tissue. These metabolites have different functions in the tissue. Choline is a marker of cellularity and cell membrane breakdown. Creatine is a marker of cellular energetics. NAA is a neuronal marker.

In the study of proton MR spectroscopic imaging of tumor an increase in choline peak, and a decrease in NAA peak has been observed [13]. Creatine has been observed to have variable amounts in tumors. Lipid and lactate are other two metabolite peaks which can be detected by ^1H MRSI. Lipid can be seen at necrotic tissue, while lactate is obtained due to lack of enough oxygenation. Although ^1H MRSI is very common and it provides a lot of information, water suppression and lipid signal problems from the fatty tissue of the brain (around scalp) are issues with this technique [14]. There are some studies for this purpose.

For instance, one study suppressed lipid to measure NAA peak accurately [14, 15], and another study implemented a reconstruction method to reduce lipid after acquiring MRS data [16].

One limitation of acquiring MRSI data for brain tumor patients is the relatively long data acquisition time. It is proportional to the number of phase encode steps (FOV) for conventional MRSI. Another common type of MR spectroscopy which is used to characterize organic structure is ^{13}C NMR. It is used to determine the type of carbon atoms in the molecule. Figure 2.4 shows sample spectra from three different MRS methods. Top left and right represent ^{13}C MRSI and ^1H MRSI data and bottom spectrum belongs to ^{31}P MRSI data.

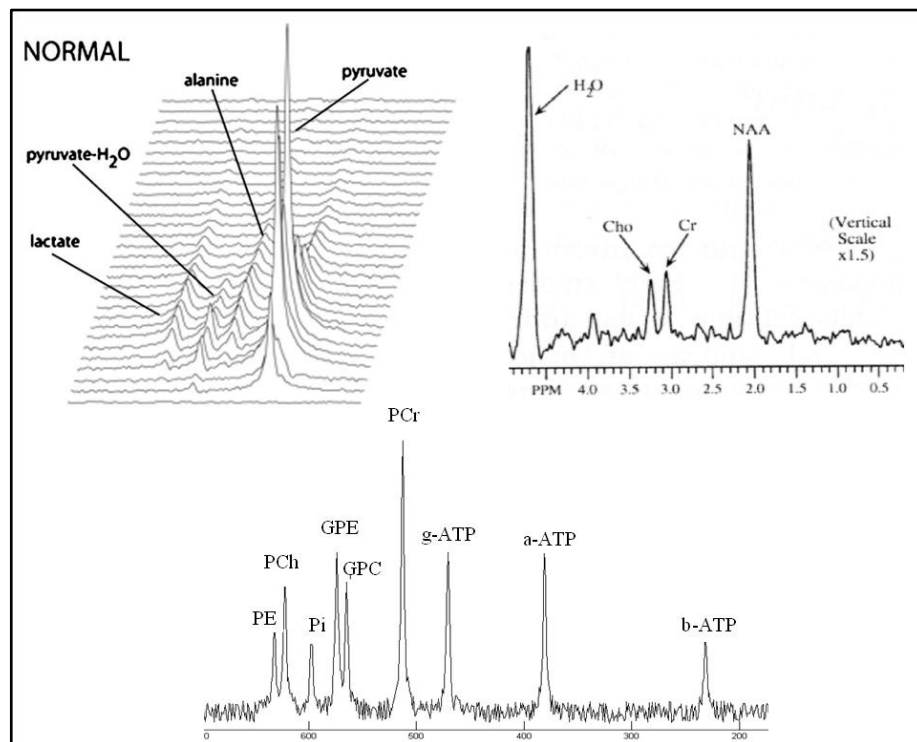


Figure 2.4 Sample spectra of ^{13}C MRSI (top left) [17], ^1H MRSI (top right) [18] and ^{31}P MRSI (bottom)

2.3 ³¹P PHOSPHORUS MAGNETIC RESONANCE SPECTROSCOPIC IMAGING

Phosphorus magnetic resonance imaging (³¹P-MRSI) is another type of non invasive MR spectroscopic imaging method that detects phosphorus in brain metabolites instead of proton. ³¹P-MRSI gives in vivo quantitative information about the energy metabolism of the brain. Also it provides oxygen state and pH value of tissue of interest [1]. Phosphocreatine (PCr), phosphorylcholine (PC), phosphorylethanolamine (PE), inorganic phosphate (Pi), glycerophosphorylcholine (GPC), glycerophosphorylethanolamine (GPE), γ -ATP, α -ATP, and β -ATP peaks are the main ones which can be detected by ³¹P-MRSI. Table 2.1 gives information about metabolite peak locations and characteristics.

Table 2.1 ³¹P MRS metabolite peak locations, and their roles in biological events

Metabolite Peak Names	Location (ppm)	Peak Characteristics
PCr	0	Considered as reference peak, a marker for phosphorylative metabolism
α -ATP	-7.5	Gives information about energetic state
β -ATP	-16	Used to estimate the level of ATP
γ -ATP	-2.4	Gives information about energetic state
PE	6.77	Takes a role in membrane synthesis, one of PME peaks
PC	6.23	Takes a role in membrane synthesis, one of PME peaks
Pi	4.8	Increases during fatigue due to breakdown of creatine phosphate
GPE	3.48	Takes a role in membrane degradation, one of PDE peaks
GPC	2.95	Takes a role in membrane degradation, one of PDE peaks

Phosphocreatine (PCr) has several characteristics. It can be seen as a singlet peak at 0 ppm, is a marker for phosphorylative metabolism, and it is considered as a reference peak in ^{31}P spectrum. Phosphorylcholine (PC) and phosphorylethanolamine (PE) are commonly called as phosphomonoesters (PME), which are produced during membrane synthesis. Glycerophosphorylcholine (GPC) and glycerophosphorylethanolamine (GPE) are produced during membrane degradation and these two peaks are called phosphodiester (PDE). Since β -ATP does not contain AMP and ADP contamination, it can be used to estimate the level of ATP. In addition, by just looking at the frequency difference between Pi and PCr metabolites in vivo, pH level could be computed using the following formula [2],

$$pH = 6.75 + \log \left[\frac{d - 3.27}{5.69 - d} \right] \quad (2.2)$$

where d is the frequency difference between PCr and Pi peaks.

In previous studies, scientists reported that phosphorus metabolite peak levels are different between healthy and brain tumors [1, 2]. When the brain tissue gets ischemic, ATP production comes from hydrolysis of PCr catalyzed by creatine kinase leading to a reduction of PCr/ β -ATP ratio in ^{31}P -MRSI [2], and the breakdown of glycogen to lactic acid which can be observed as the lactate peak in proton MR spectra [3]. Pi increases at ischemia state because of increased ATP hydrolysis and this is not matched by ATP synthesis which leads an increase in Pi/PCr ratio [1]. A significant reduction in PCr/Pi peak ratio and an increase of pH levels in brain tissue were reported by Hubesh et al [1]. An alkaline environment and a decrease of PCr and PDE metabolite peaks for meningiomas were reported by Maintz et al. and a slight alkalization (pH=7.09) and more than a factor of two reduction in the ratio of PDE/ α -ATP peaks for low grade gliomas were observed by them [2]. Figure 2.5 shows phosphorus MR spectra of a healthy volunteer. Signals were acquired from the brain. Main peaks can be seen clearly. Figure 2.6 represents MR images of a brain tumor patient and AMARES quantification of the ^{31}P MRS data acquired from a single voxel.

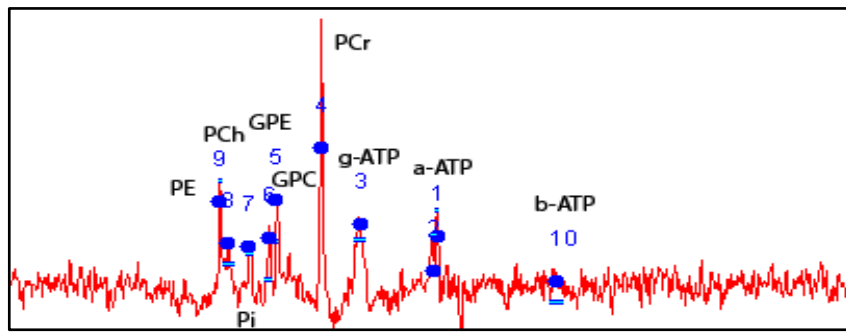


Figure 2.5 ^{31}P MRSI spectra from a healthy volunteer. Main ^{31}P spectrum metabolite peaks are clearly shown

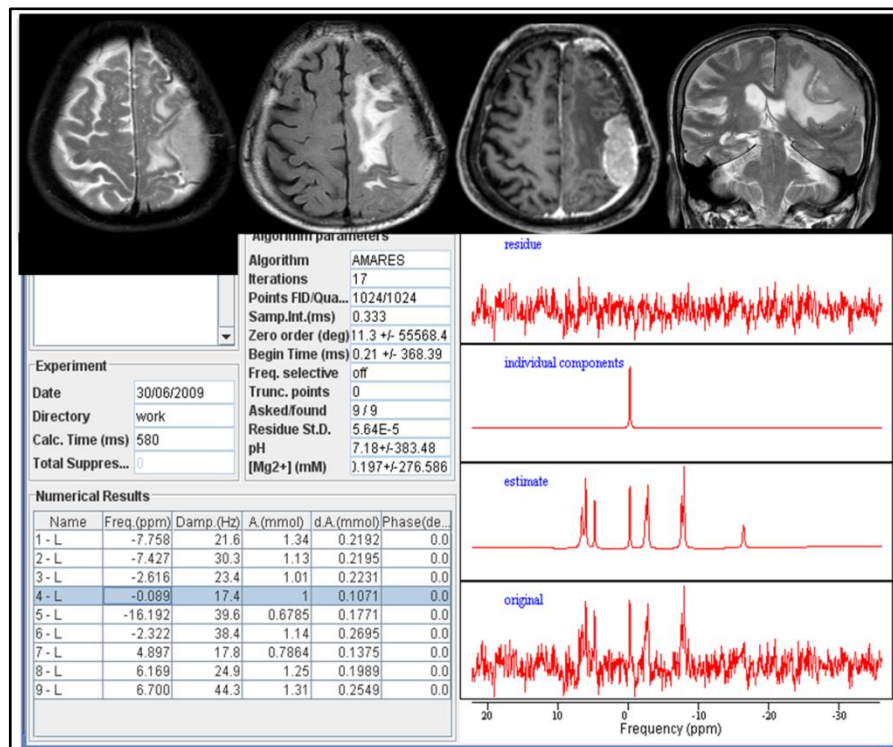


Figure 2.6 MR anatomical image of a brain tumor patient and quantification of ^{31}P MRSI data in AMARES tool within jMRUI

2.4 IMAGE SELECTED IN VIVO SPECTROSCOPY

Image Selected in vivo Spectroscopy (ISIS) is a multi shot method which uses a combination of eight pulses. Volume of interest (VOI) is pre selected and based on MRI scan, it is excited repeatedly. This method has been applied to phosphorus and proton MR

spectroscopy. ISIS does not have T_2 weighting which is a nice advantage of it. On the other hand, eight phase cycles are required for a voxel localization might be a problem for shimming purposes.

ISIS is a data acquisition method which provides a facility of using low TE (echo time) values and this helps out acquiring fast attenuated MR signals [19]. Since phosphorus contain metabolites have short T_2 values, ISIS became a common data acquisition method in ^{31}P MRSI. ISIS acquires free induction decay (FID) signal as a result of one RF pulse instead of acquiring echo signal which needs two RF pulses and longer TE times. ISIS method requires two or more distinct signal measurements to receive MR signal from the area of interest and using a proper formula this MR signal could be separated. Essentially, ISIS is a single voxel MR spectroscopy technique, but using 1D ISIS method one slice can be selected, using 2D ISIS one column can be selected and using 3D ISIS method a voxel can be selected.

Figure 2.7 shows 1D ISIS method to select one slice which requires two different measurements. In the first measurement, applying 90° RF pulse flips net magnetization into the XY plane and a signal is collected from the slice and the surrounding tissue. In the second measurement, 180° RF pulse is applied first at the same time with a gradient to select the slice before 90° RF pulse is applied. 180° RF pulse reverses the net magnetization within the slice. Afterward, a 90° RF pulse is applied and this flips the signals which come from the selected slice and signals from surrounding in opposite directions into XY plane, and the signal is acquired. Subtraction of these two measurements divided by two gives an approximate value of the MR signal from the slice of interest.

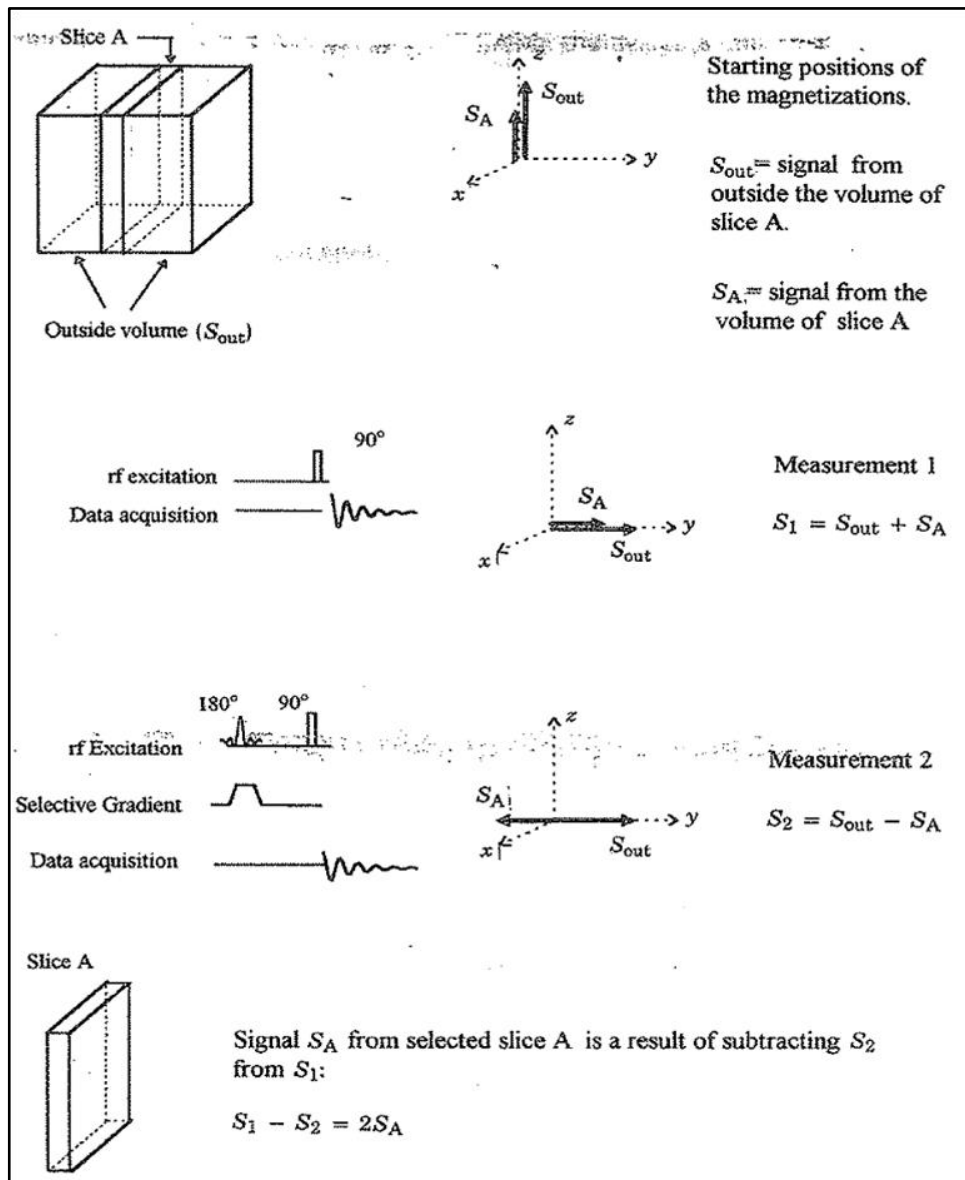


Figure 2.7 One dimensional ISIS with two measurements which localizes the spectrum to a slice [18]

2D ISIS method requires two different directed gradients and four different measurements to achieve signal localization. Figure 2.8 represents 2D ISIS method with four measurements.

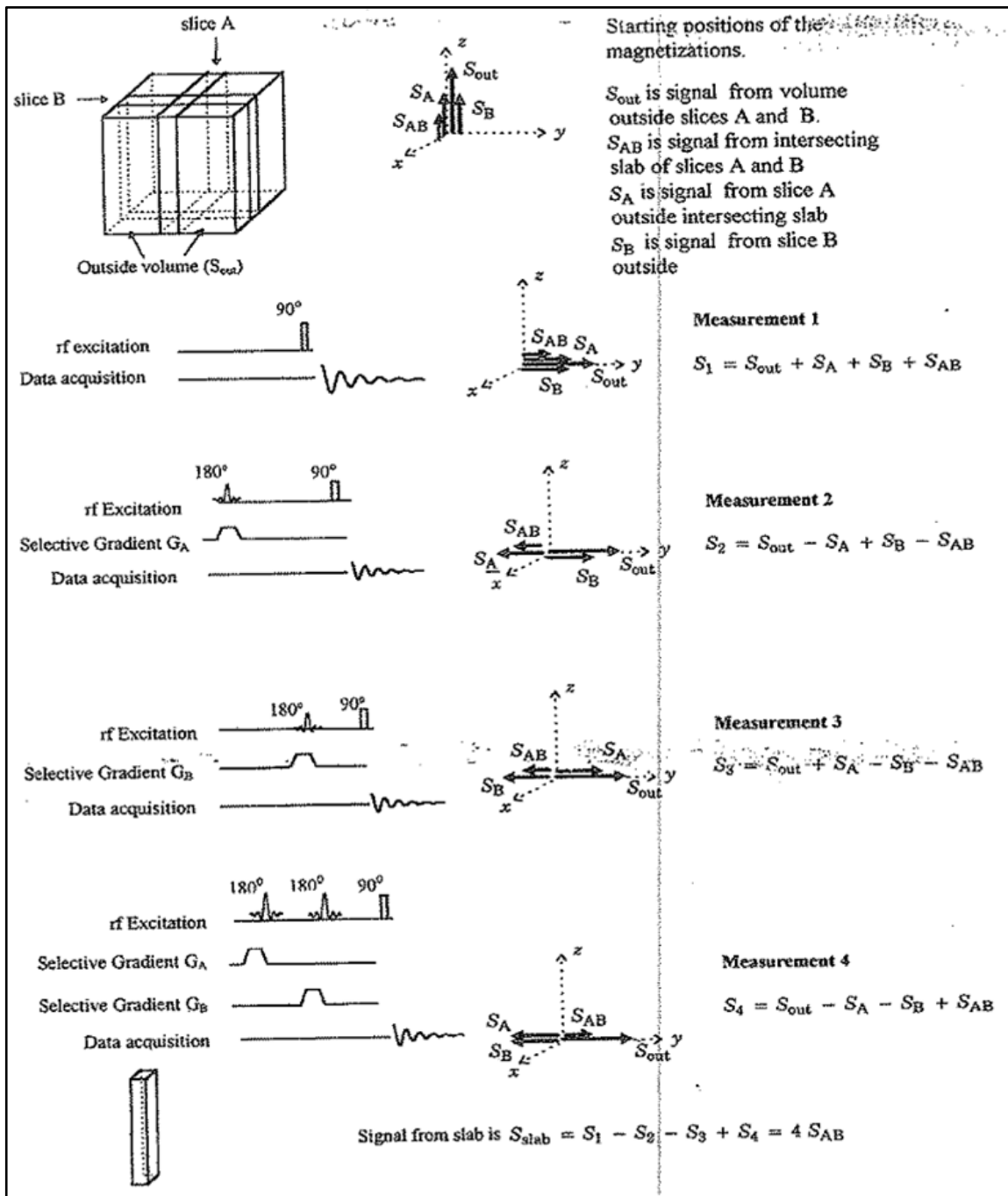


Figure 2.8 Two dimensional ISIS with four measurements and it localizes the spectrum to a column [18]

In 3D ISIS method, three different gradient directions and eight different measurements are needed. Figure 2.9 shows gradient combinations of eight signals for three dimensional ISIS method for a selection of a voxel which occurs at the intersection of A,B,C slices on x, y, z axes. G_A , G_B , G_C are slice selective gradients to select A, B, and C slices, respectively.

They are used simultaneously with 180° inversion pulses. The magnetization in slice A is inverted during measurements 2, 5, 6, and 8. The magnetization in slice B is inverted during measurements 3, 5, 7 and 8. The magnetization in slice C is inverted during measurements 4, 6, 7, and 8. Signal from the voxel is obtained by combining signals from these eight measurements according to the following formula,

$$S_1 - S_2 - S_3 - S_4 + S_5 + S_6 + S_7 - S_8 = 8S_{ABC} \quad (2.3)$$

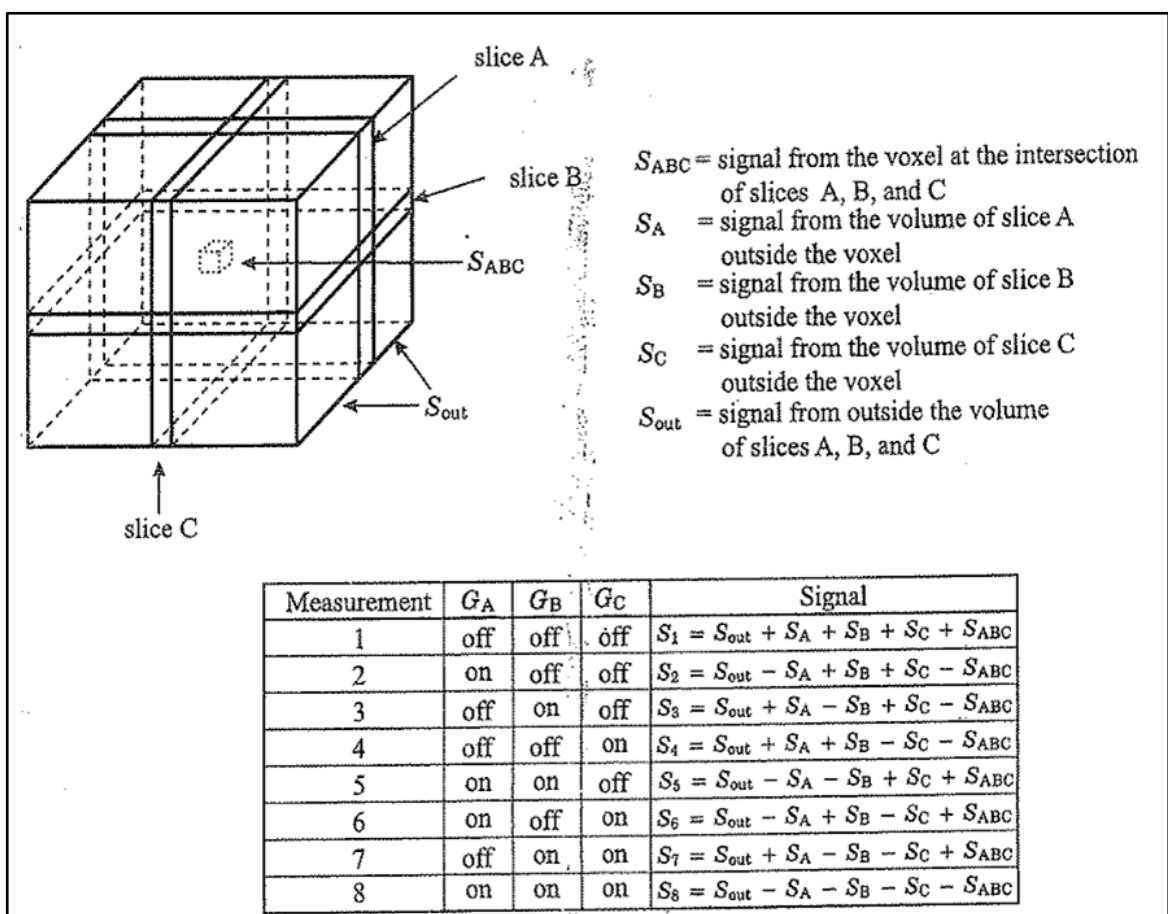


Figure 2.9 Three dimensional ISIS method which needs eight measurements to localize the spectrum to the voxel, S_{ABC} [18]

2.5 WAVELET TRANSFORM

The first criterion of compressed sensing algorithm that needs to be satisfied is the sparsity of the undersampled signal in a transform domain. The Wavelet transform is a computational tool which is used for signal and image processing applications. Wavelet transform can also reduce noise. There are two types of Wavelet transform. One is easily reversible, which is if we have original signal it can be easily recovered after it has transformed. This type is used for image compression and reducing noise.

In general, first the Wavelet transform of the image is computed, then the Wavelet representation is modified properly, finally the Wavelet transform is inverted to obtain a new image. The second type is for signal analysis for EEG studies or similar applications. The basic Wavelet transform is the Haar transform which was found by Alfred Haar (1910) and the latest Wavelet transform was found by Ingrid Daubechies (1998). Wavelet transform is used in MRI to get sparse images. In Fourier analysis, each function is represented as a summation of sines and cosines. However, in Wavelet analysis, each function can be divided into its approximation and details. It is represented as a summation and details of a mother basis function and its scaled and dilated versions [20]. Figure 2.10 shows 2D Wavelet transform of an image which was performed using MATLAB.

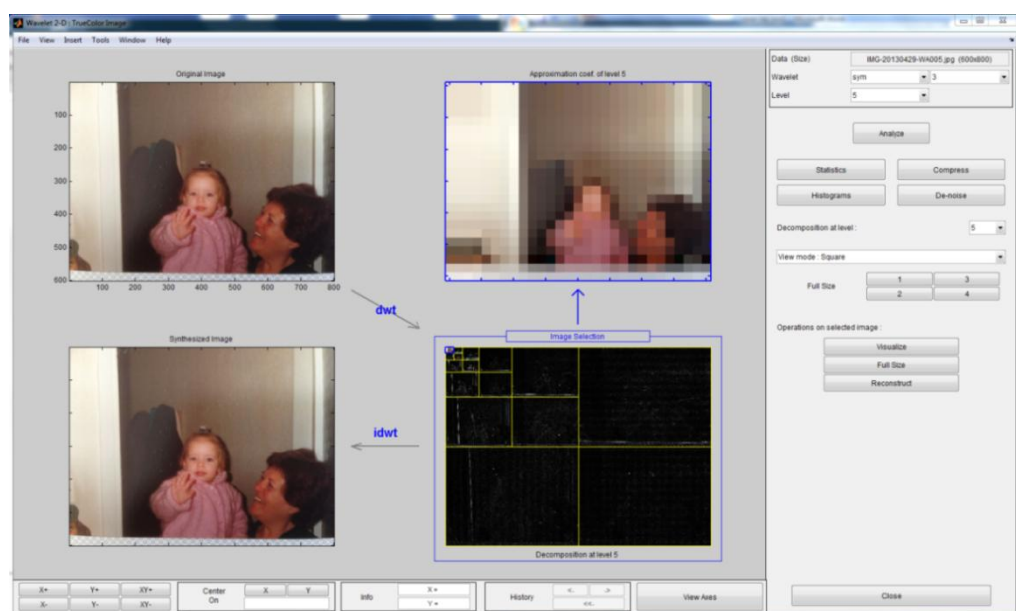


Figure 2.10 An example of 2D Wavelet transform using Wavelet toolbox in MATLAB

2.6 COMPRESSED SENSING METHOD

Compressed sensing is the latest fast MR acquisition method which can provide an exact reconstruction of sparsely undersampled MR signals. The basic formula of this technique was firstly found by Dr. Emmanuel Candes while he was conducting an experiment on noise reduction of Shepp-Logan phantom. They provided that the l_1 norm reduction gives a perfect image reconstruction [21].

Compressed sensing has three criteria. Those criteria have to be satisfied for using compressed sensing for reconstruction. First, the signal needs to be sparse in a transform domain. So, it should have a few non zero components in transform domain. Second requirement is that the signal should be randomly undersampled. The resultant image should then have incoherent aliasing pattern. Finally, there should be a nonlinear reconstruction method. In this case conjugate gradient method was used to find an approximate solution for an ill-posed problem.

Lustig et al. applied the first application of compressed sensing for faster MR angiography and spin echo images [6]. Later, Hu et al. applied compressed sensing for rapid ^{13}C MR spectroscopic imaging [7, 8]. Since MRS signals are naturally sparse, they have a few non-zero components along the spectral bandwidth (only certain frequencies). In addition, a sparse MRS signal can be specified with a few large Wavelet components, which is also first requirement to implement compressed sensing reconstruction [7]. We can formulate compressed sensing of randomly selected spectral data in (k, t) domain as,

$$\begin{aligned} & \min (\|\psi(m)\|_1) \\ & \text{s. t. } \|F_a(m) - y\|_2 < \varepsilon \end{aligned} \tag{2.4}$$

Equation (2.4) gives the formula of compressed sensing method. m indicates an approximate solution, $\psi(m)$ is Wavelet transform of this solution, $\|\cdot\|_1$ is the l_1 norm, F_a represents a random undersampling operator in Fourier domain, y indicates the original Fourier domain samples and ε indicates an error at noise level. l_1 norm of the Wavelet transform should be minimum. Equation 2.5 shows l_1 calculation,

$$\|x(i)\|_1 = \sum_i |x(i)| \quad (2.5)$$

Equation (2.4) points out that the undersampled Fourier transform of accurate solution and undersampled Fourier transform of original data should be in good agreement. The solution should also be sparse to be compressed with Wavelet transform. These sparsity and discrepancy criteria can be transformed to Lagrange form and can be rewritten as an optimization problem as,

$$\min_m (\|F_a(m) - y\|_2 + \lambda \|\psi(m)\|_1) \quad (2.6)$$

Due to limited undersampling in Fourier domain, MR reconstruction problem is an underdetermined problem and this problem could have multiple solutions. This cause MR reconstruction problem to be ill posed [22]. For the solution of ill posed problems we need to search approximate solution instead of accurate solution or we should use a priori information. Another way is to use regularization techniques [23]. Generally, conjugate gradient regularization method is used to search for a solution of compressed sensing reconstruction problem. This method will be explained in detail at the next section.

2.7 CONJUGATE GRADIENT METHOD

Conjugate gradient method [24] is an iterative method and it can be implemented for sparse systems which take long time to handle with direct methods. This method is also widely used for unconstrained optimization problems. Conjugate gradient method uses the following equation,

$$\eta_x = \frac{1}{2} x^T A x - b^T x + c \quad (2.7)$$

which is a quadratic function of simple linear equation $Ax=b$. A should be a real positive definite matrix. Conjugate gradient method is used to find unknown x value which minimizes the quadratic equation. Unknown x is also the solution of $Ax=b$ equation. The minimum value of an $f(x)$ function is where its gradient value is equal to zero. The gradient of $f(x)$ is a vector which shows the most increased direction of $f(x)$ at any given x value

[25]. Gradient of η_x function can be found by applying simple matrix derivation rules as $Ax=b$,

$$\begin{aligned}\frac{d}{dx}(x^T Ax) &= 2Ax \\ \frac{d}{dx}(b^T x) &= b\end{aligned}\tag{2.8}$$

In this case, the point where gradient of η_x function becomes zero is also a solution of $Ax=b$ linear equation. An x value which is least different from the minimum value of quadratic of η_x function can be calculated with steepest descent method [25].

Conjugate gradient method starts from a randomly selected x_0 value and it continues iteratively in the direction of the fastest reduction of Ax_i-b difference to reach the best solution. Since the gradient of a function shows the direction of the fastest increase, the steepest descent algorithm takes steps in the direction of the negative gradient of η_x function. The negative gradient of η_x function ($r_i=b-Ax_i$) which is actually a difference between b value (original measurements) and Ax_i value (at any given x_i value) can be seen. The steepest descent algorithm finds the next x_i value by starting from the point of the random x_0 value, and adding the error of the difference occurred when x_i is inserted into the function, r_i , multiplied by the α weight value. The iterative processing could be defined by,

$$x_{i+1} = x_i + \alpha r_i\tag{2.9}$$

Consecutive difference values could be calculated as,

$$r_{i+1} = r_i + \alpha A r_i\tag{2.10}$$

The steepest descent algorithm can take consecutive steps in the same direction and this can prolong the convergence time of the algorithm. Conjugate gradient method is an improved version of steepest descent method. In conjugate gradient method consecutive steps are perpendicular to each other which reaches the solution in a shorter time. If p_i and

p_{i+1} are consecutive two search direction, they should be A perpendicular to each other in conjugate gradient method,

$$p_k \cdot A \cdot p_{k+1} = 0 \quad (2.11)$$

New search direction can be calculated depending on the difference between the previous search direction and difference,

$$p_{i+1} = r_{i+1} + \beta_i p_i \quad (2.12)$$

β value defined here is second weighting factor which is used in conjugate gradient method and also it is used to find the direction of the next search for a solution. Iterative solution of x_i value in conjugate gradient method is shown below,

$$x_{i+1} = x_i + \alpha_i p_i \quad (2.13)$$

Residual error of next step can be measured by,

$$\begin{aligned} r_{i+1} &= b - Ax_{i+1} \\ &= b - A(x_i + \alpha_i p_i) \\ &= r_i - \alpha_i A p_i \end{aligned} \quad (2.14)$$

Weighting factor α can be calculated using the above equation (consecutive residual errors are perpendicular to each other),

$$\begin{aligned} (r_i - \alpha_i A p_i) r_i &= 0 \\ \alpha_i &= r_i \cdot r_i / r_i \cdot A \cdot p_i \end{aligned} \quad (2.15)$$

Weighting factor β can be calculated with using the information that consecutive search directions are A perpendicular,

$$p_{i+1} \cdot A \cdot p_i = 0 \quad (2.16)$$

$$(r_{i+1} + \beta_i p_i) \cdot A \cdot p_i = 0$$

$$\beta_i = -r_{i+1} \cdot A \cdot p_i / p_i \cdot A \cdot p_i$$

For each iteration, if the residual error reduces to a minimum value then we can say conjugate gradient method approaches to a convergence. However residual error begins to increase or the difference between two consecutive residual error values is 15%-20% higher than the previous error value, iteration stops and it assumes that it found the solution of $Ax=b$ function [25].

2.8 STATISTICAL METHODS

2.8.1 Bland Altman Method

Bland Altman is a statistical test that compares data acquired from two different measurement techniques of the same thing. The difference of the two measurements is plotted against the mean of the two measurements at all the points. The mean and plus and minus 2 standard deviation of the differences are also plotted on the same figure. For accepting that there is no difference between the two techniques, the difference of the two measurements should remain within plus or minus two standard deviations of the mean difference [26]. Each of the samples are plotted on the graph by assigning the mean of two measurements on the x axis and the difference between the two measurements on the y axis. Following formula gives Cartesian coordinates of a sample S, with S_1 and S_2 values defined by two measurements,

$$S(x, y) = \left(\frac{S_1 + S_2}{2}, (S_1 - S_2) \right) \quad (2.17)$$

2.8.2 Wilcoxon Signed Rank Sum Test

Wilcoxon ranksum test is a non-parametric test for the null hypothesis that two populations are the same. Particularly the test checks if one population tends to have larger values than the other one. It is a non-parametric method, which is equivalent to parametric t-test. T-test

is used to compare two different groups whose values are normally distributed. Wilcoxon ranksum test can be applicable when two criteria are satisfied. First, dependent values should be measured on ordinal or interval/ratio scale. Second, if the values are independent, it should be composed of two classes which are connected groups or coherent pairs [26].

First, all of the observations are arranged into a single ranked sequence. For ranking, all the data points are considered as if they belong to the same category, and are ranked together.

First method is a direct method which can be used for small samples. Assume that sample 1 sample 2 are two groups that we would like to compare. In sample 1, for each observation we count the number of observations in which sample 2 have a smaller rank. The sum of these numbers is called U.

The second method is used for larger samples. First the ranks for the observations of sample 1 are summed up. Since the addition of all the ranks equals to $N(N+1)/2$ (N is total number of observations), the sum of ranks from sample 2 is limited. Then following formula can be used for next calculations,

$$U_1 = R_1 - \frac{n_1(n_1 + 1)}{2} \quad (2.18)$$

where n_1 represents the sample size for sample 1 and R_1 denotes the sum of the ranks in sample 1. Equally valid formula for U is,

$$U_2 = R_2 - \frac{n_2(n_2 + 1)}{2} \quad (2.19)$$

The sum of the two values, U_1 and U_2 , is given as,

$$U_1 + U_2 = R_1 - \frac{n_1(n_1 + 1)}{2} + R_2 - \frac{n_2(n_2 + 1)}{2} \quad (2.20)$$

Using the knowledge of $R_1+R_2=N(N+1)/2$ and $N=n_1+n_2$, the sum is acquired as,

$$U_1+U_2 = n_1n_2 \quad (2.21)$$

3. MATERIAL AND METHODS

3.1 DATA ACQUISITION

A volunteer, who provided informed consent, was scanned on a 3T MR scanner (Philips Medical Systems, Best, Netherlands). ^{31}P surface coil which had a disk at the center containing methylphosphonic acid and water was used in this study. The coil was used as a localization reference. TFE survey images were acquired using body coil, the following parameters were used, repetition time (TR)=75 ms, encoding time (TE)=5ms, and flip angle was set to 30° .

Image selected in vivo spectroscopy (ISIS) method was used to obtain phosphorus MR spectrum from frontoparietal lobe of a volunteer. The following parameters were used in ISIS, TR=5s, 128 averages, spectral bandwidth=3000 Hz, Dwell time was 0.333ms, 1024 points were acquired, voxel size was 27cc for a total scan time of 11 minutes.

3.2 DATA PROCESSING

^{31}P MR spectrum acquired from a volunteer was processed using a 10 Hz gaussian filter to reduce noise, then phase correction was applied, and baseline was removed with jMRUI software [27]. Metabolite peaks were quantified using AMARES [27] within jMRUI. The amplitude and frequency factors which were denoted by (a) and (f) respectively, were calculated for each peak k. These parameters were used to create a ^{31}P spectrum of a healthy voxel using the following formula,

$$y_n = \sum_k a_k e^{-(d_k + i2\pi f_k)t_n} \quad (3.1)$$

where d_k was set to 30 Hz for all the peaks in MATLAB (The Mathworks Inc., Natick, MA). Similarly, a ^{31}P spectrum of a tumor voxel was created using (0.49, 1.0, 1.0, 1.0, 2.16, 1.86, 1.47, 2.06, 2.63) times the peak amplitudes of the healthy ^{31}P spectrum for the PCr, γ -ATP, α -ATP, β -ATP, GPC, GPE, Pi, PC and PE peaks, respectively. A 2D 32x32

voxels ^{31}P MRSI dataset was created using both tumor (at the top left, 10 by 10 voxels) and healthy (rest of the array) ^{31}P spectra.

A random undersampling pattern was created in MATLAB to satisfy one criteria of compressed sensing method. Figure 3.1 shows the 2D sampling mask for one of the frequency points. Mask was implemented to k-space of ^{31}P -MRSI dataset to reduce k-space along x by a reduction factor of $R=2.23$. Because of SNR concerns, the central two lines of k-space were preserved [8].

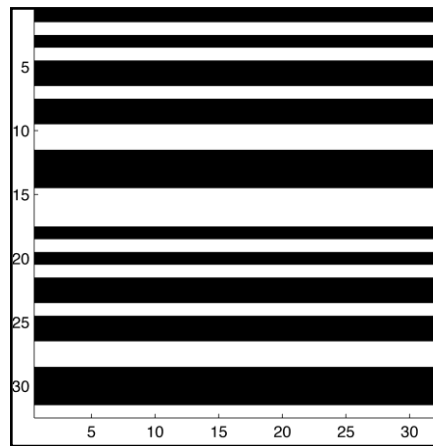


Figure 3.1 The random undersampling pattern for one of the frequency points in k-space.

In total, %56.25 of all the k-space points were set to zero ($R=2.23$)

Randomly undersampled ^{31}P -MRSI dataset was inverse Fourier transformed along k_y . Sparse MRI software package was used to reconstruct k_x -f data for each y point [6]. Flowchart of data preparation process could be seen in Figure 3.2. l_1 -norm and total variation weights were entered as 0.01 based on experiments. Sparsifying transform was 1D length-4 Daubechies Wavelet transform.

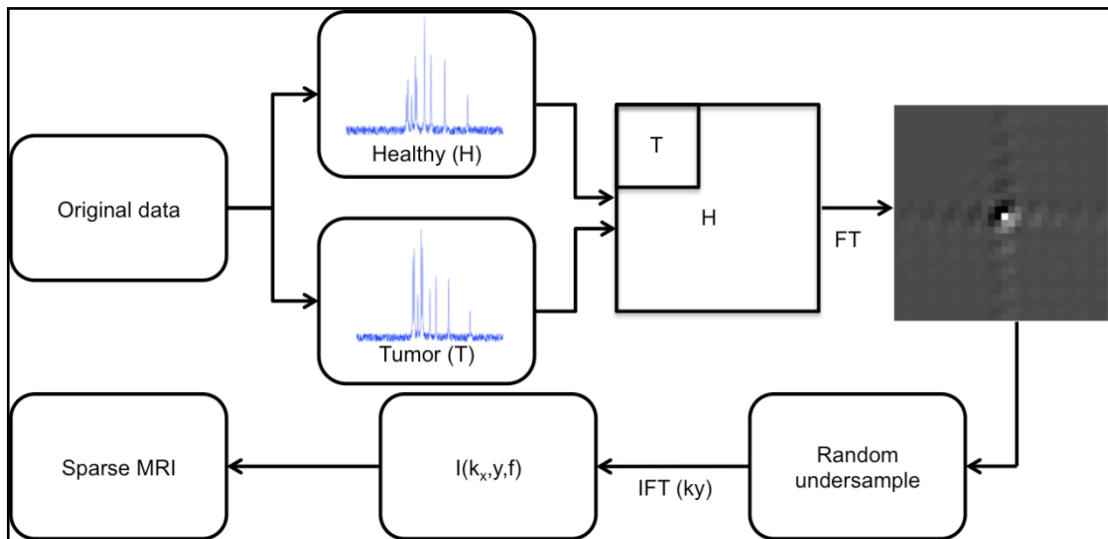


Figure 3.2 The flowchart of ^{31}P MRSI data preparation scheme

3.3 SPARSE MRI

Sparse MRI is a compressed sensing reconstruction software package, which was written by Lustig et al. [6]. This software package was written in MATLAB and it uses WaveLab tool. In the theory of compressed sensing method, sparse images were recovered from randomly undersampled k-space data, and Sparse MRI can implement this method by using an appropriate nonlinear recovery scheme. Random undersampling reconstruction adds noise like interference to the image. Reconstruction was performed by minimizing the l_1 norm of the transformed image and discrepancy. For optimization problem Sparse MRI uses a nonlinear regularization method, which is conjugate gradient method. Lustig et al. first implemented this software to accelerate acquisition for multislice fast spin echo brain imaging and 3D contrast enhanced angiography.

3.4 DATA ANALYSIS

Two statistical tests were used to analyze the results, Bland Altman and Ranksum tests. A Bland Altman statistical test was used to detect if there was any significant differences between mean PCr/PE, PCr/ β -ATP, Pi/PCr ratios of the original and compressed sensing applied phosphorus MRS datasets for both tumor and healthy regions. The difference

between all the pairs of a given peak ratio calculated from the compressed sensing and original datasets was used for Bland Altman method.

The mean difference, measure of bias between the two observations, and also standard deviation of it were calculated. For each point, the difference against the mean of the two observations was plotted. If there were no outliers below or above two standard deviations of the mean difference, that meant two observations were in good agreement.

A ranksum test was used to see if SNR of PCr, Pi and β -ATP peaks were different between tumor and healthy regions for the original and compressed sensing ^{31}P -MRSI datasets. $p < 0.05$ value was considered as significant.

4. RESULTS

^{31}P MR spectra of six voxels from the original and compressed sensing datasets are represented in Figure 4.1. The top three voxels belong to tumor spectra, and the lower three voxels belong to healthy spectra. Tumor and healthy spectral regions were clearly separable in both original and compressed sensing reconstructed datasets. Tumor spectra had lower PCr, and higher PME, PDE and Pi peaks which can be easily distinguished. ATP peak levels were quite similar between both regions, as intended in this simulation.

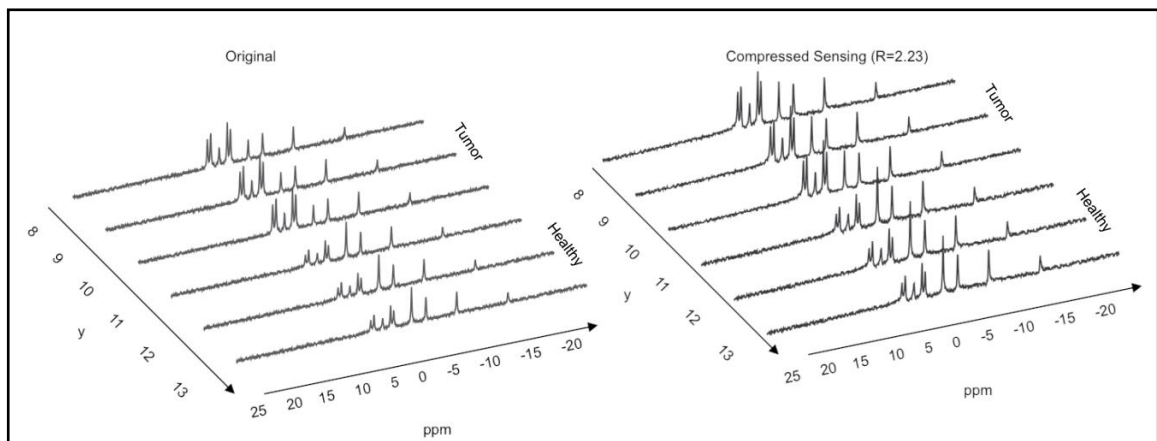


Figure 4.1 Phosphorus MR spectra of six voxels for original (left) and compressed sensing (right) datasets

Table 4.1 gives ratios of Pi/PCr, PCr/ β -ATP, and PCr/PE peaks in tumor and healthy regions for the original and compressed sensing reconstructed datasets. As seen clearly, tumor regions had higher Pi/PCr, and lower PCr/ β -ATP and PCr/PE metabolite ratios than the healthy regions for both compressed sensing and original datasets.

Table 4.1 Metabolite Ratios In Tumor And Healthy Regions For The Original (O) And Compressed Sensing (CS) Datasets

Metabolite Ratios (mean±std)		<i>Pi/PCr</i>	<i>PCr/β-ATP</i>	<i>PCr/PE</i>
CS	Tumor	0.80±0.03	2.04±0.07	0.77±0.04
	Healthy	0.34±2.4e-05	3.09±4.2e-04	2.68±3.4e-04
O	Tumor	1.05±0	1.70±0	0.56±0
	Healthy	0.35±0	3.06±0	2.80±0

Table 4.2 represents the results of the Bland Altman statistical test which measures the bias and the variation of the peak ratios for the original and compressed sensing datasets. For healthy regions, metabolite ratios were similar between the original and compressed sensing datasets and the mean difference (bias) was 0.01, 0.03, and 0.13 for Pi/PCr, PCr/β-ATP and PCr/PE metabolite ratios, respectively. However, tumor regions had higher bias than healthy regions. There were no outliers in the tumor region which indicate that the variation of the differences between the peak ratios was low in tumor region. In contrast there were around 20 outliers in the healthy region for Pi/PCr, PCr/β-ATP and PCr/PE metabolite ratios due to low standard deviation in this region.

Table 4.2 Bland Altman Test Results For The Difference Of Peak Ratios In The Original And Compressed Sensing Datasets For Tumor And Healthy Regions

Bland Altman Test Results		<i>Pi/PCr</i>	<i>PCr/β-ATP</i>	<i>PCr/PE</i>
Tumor	# outliers	0	0	0
	mean(difference)	0.25	0.34	0.21
	std(difference)	0.03	0.07	0.04
Healthy	# outliers	20	27	20
	mean(difference)	0.01	0.03	0.13
	std(difference)	2.45e-5	4.16e-4	3.53e-4

Figures 4.2 to 4.7 represent Bland Altman statistical test plots of metabolite peaks for healthy and tumor regions. Bland Altman test was used to calculate the bias and the variation of the peak ratios for the original and compressed sensing datasets. Figure 4.2 shows Bland Altman test result of Pi and PCr metabolite peak ratios for healthy regions. Metabolite ratios were similar between compressed sensing and the original datasets and the bias of Pi/PCr was 0.01. Figure 4.3 shows Bland Altman test result of Pi and PCr metabolite peak ratios for tumor regions which had higher bias than healthy regions. Figure 4.4 shows Bland Altman test result of PCr and β -ATP metabolite peak ratios for healthy regions. Metabolite ratios were similar between compressed sensing and the original datasets and the mean difference of PCr/ β -ATP was 0.03. Figure 4.5 shows Bland Altman test result of PCr and β -ATP metabolite peak ratios for tumor regions, which had higher bias than healthy regions. Figure 4.6 shows Bland Altman test result of PCr and PE metabolite peak ratios for healthy regions. Metabolite ratios were similar between compressed sensing and the original datasets and the mean difference (bias) of PCr/PE was 0.13. Figure 4.7 shows Bland Altman test result of PCr and PE metabolite peak ratios for tumor regions, which had higher bias than healthy regions. There were no outliers in the tumor region. The results point out that the variation of the differences between the peak ratios were lower in the tumor region.

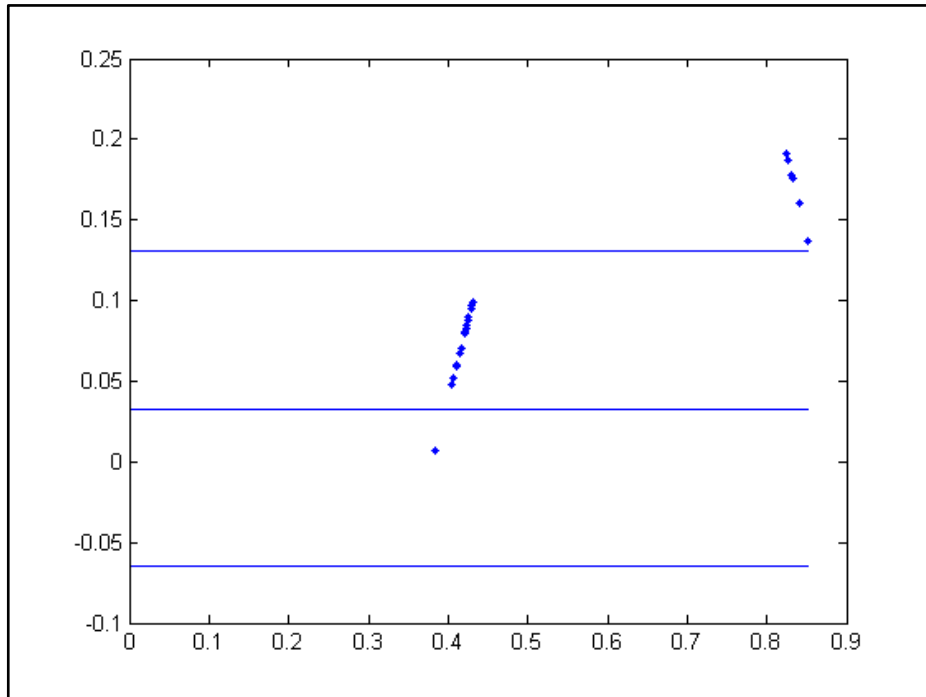


Figure 4.2 Bland Altman statistical test plot of Pi and PCr peak ratios for healthy region

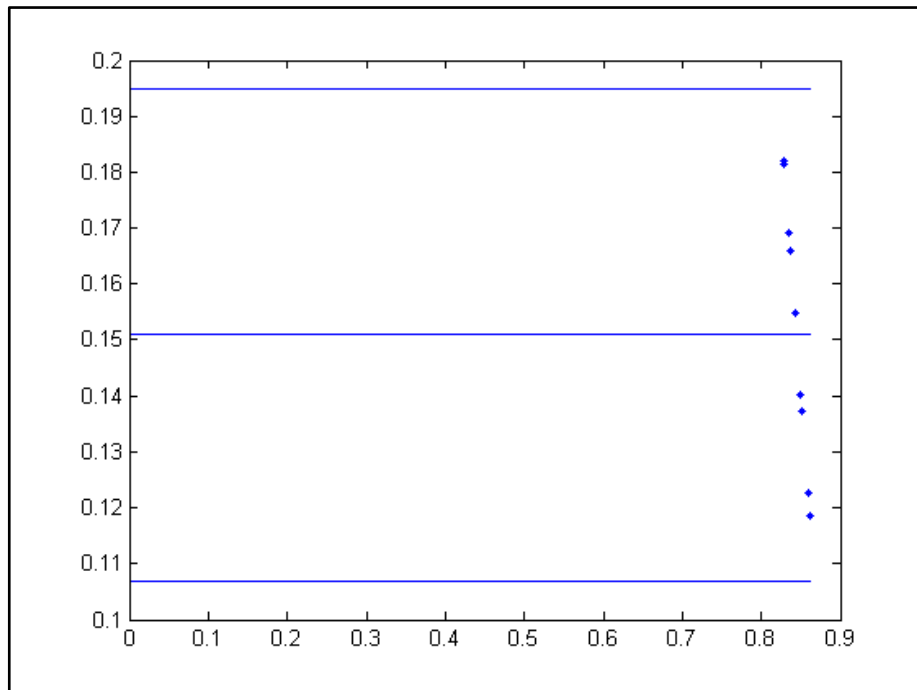


Figure 4.3 Bland Altman statistical test plot of Pi and PCr peak ratios for tumor region (no outliers)

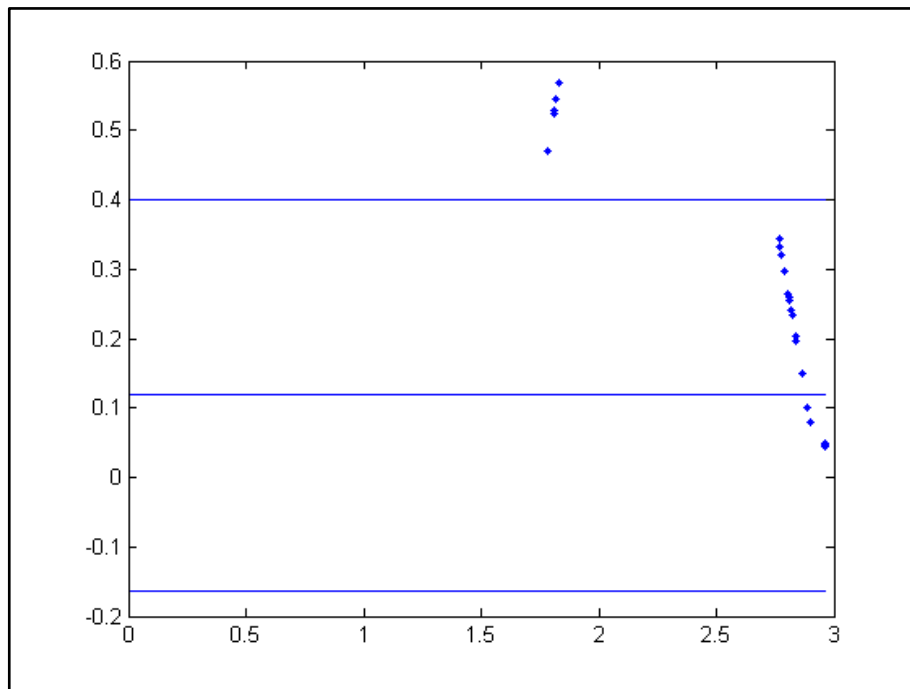


Figure 4.4 Bland Altman statistical test plot of PCr and β -ATP peak ratios for healthy region

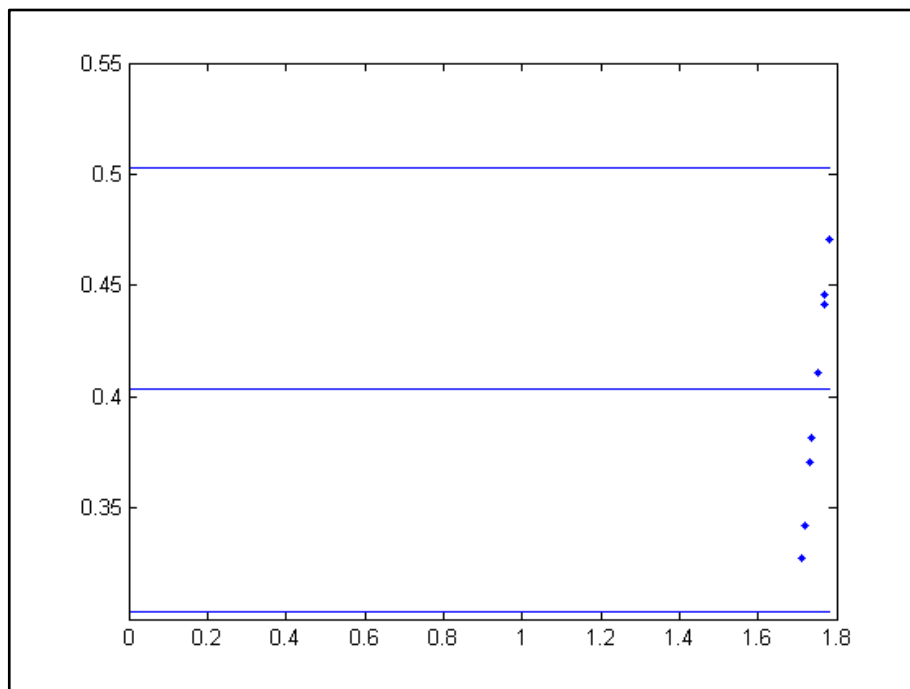


Figure 4.5 Bland Altman statistical test plot of PCr and β -ATP peak ratios for tumor region (no outliers)

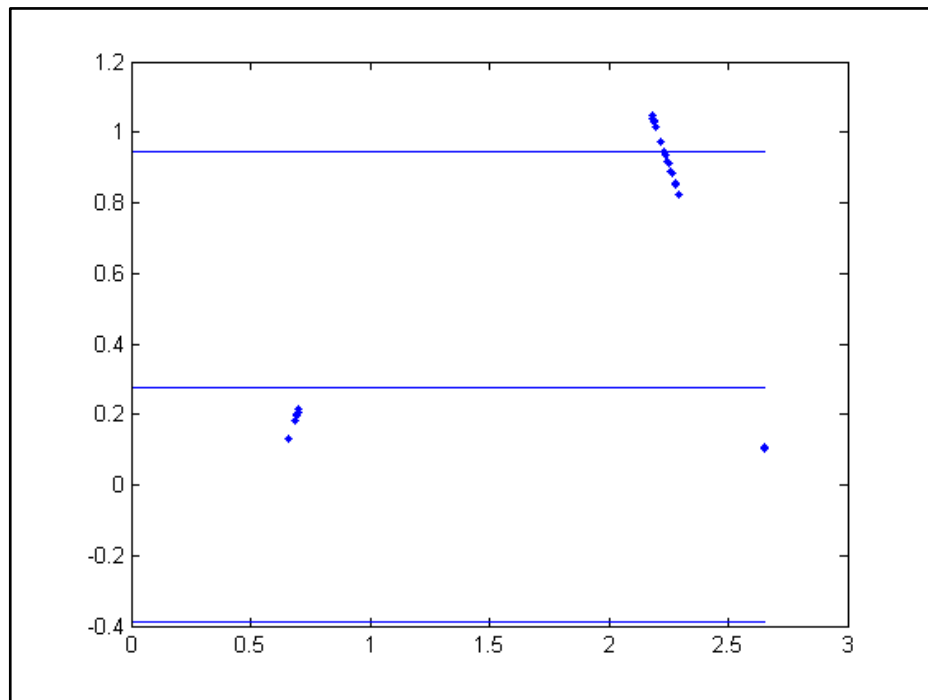


Figure 4.6 Bland Altman statistical test plot of PCr and PE peak ratios for healthy region

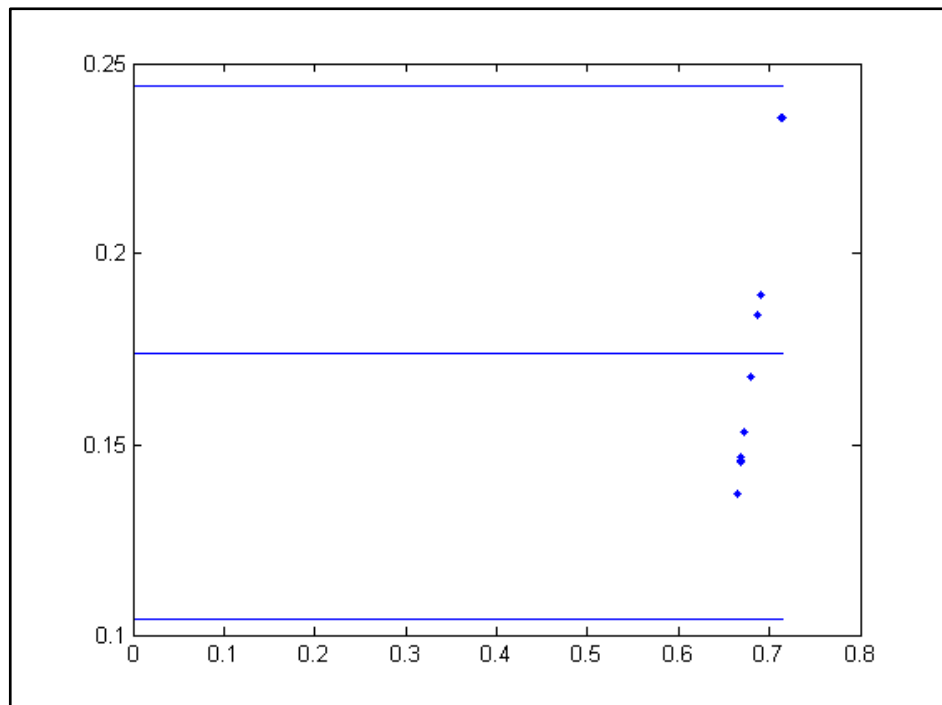


Figure 4.7 Bland Altman statistical test plot of PCr and PE peak ratios for tumor region
(no outliers)

Table 4.3 demonstrates SNR of PCr, Pi, and β -ATP metabolite peaks in tumor and healthy regions and SNR ratios between these two regions for the original and compressed sensing datasets. SNR of all metabolite peaks were higher due to denoising effect of compressed sensing reconstruction. Tumor regions had a higher denoising than healthy regions. This resulted in higher tumor/healthy SNR ratios in compressed sensing dataset than the original dataset.

Table 4.3 SNR Values Of Metabolite Ratios In Tumor And Healthy Regions And Their Ratios Of The Original (O) And Compressed Sensing (CS) Datasets

SNR (mean \pm std)		<i>Tumor</i>	<i>Healthy</i>	<i>Tumor/Healthy</i>
CS	PCr	46.13 \pm 3.11	57.53 \pm 0.06	0.80
	Pi	37.03 \pm 1.76	19.46 \pm 0.02	1.90
	β -ATP	22.59 \pm 1.21	18.60 \pm 0.02	1.21
O	PCr	19.73 \pm 0	42.68 \pm 0	0.46
	Pi	20.77 \pm 0	14.77 \pm 0	1.41
	β -ATP	11.62 \pm 0	13.95 \pm 0	0.83

The results of the ranksum test indicate that SNR of PCr was statistically significantly lower ($p < 0.001$), but SNR of Pi was significantly higher ($p < 0.001$) in tumor regions than healthy regions for both datasets. Although β -ATP SNR levels were quite similar in tumor and healthy regions, there was a statistically significant difference between them ($p < 0.001$) due to the higher number of voxels considered.

Table 4.4 shows the ratios of tumor over healthy mean peak heights of PCr, Pi and β -ATP metabolite peaks for the original and compressed sensing datasets. The tumor spectrum was simulated to have 0.49, 1.0, and 1.47 times the peak amplitudes of the healthy spectrum for the PCr, β -ATP, and Pi peaks, respectively. Both datasets had similar ratio of tumor over healthy mean peak heights.

Table 4.4 Ratio of Tumor over Healthy Mean Peak Heights for each of metabolite peaks in both datasets.

Ratio of Tumor/Healthy Mean Peak Heights	<i>PCr</i>	<i>Pi</i>	<i>β-ATP</i>
Compressed Sensing	0.59	1.40	0.89
Original	0.52	1.59	0.94

5. DISCUSSION

This simulation study examined the usage of compressed sensing reconstruction technique for reducing the scan time for accelerating ^{31}P MR spectroscopic imaging. Results have shown that SNR of compressed sensing applied dataset was higher than the original dataset due to compressed sensing denoising effect. However, peak height ratios were quite similar between compressed sensing and original datasets. Compressed sensing method for ^{31}P MRSI could be further developed by acquiring fewer k-space lines or changing random undersampling pattern. Future studies will investigate the effectiveness compressed sensing method for shortening the scan time of ^{31}P MR spectroscopic imaging in brain tumors.

6. REFERENCES

1. Hubsch, B., et al., *P-31 MR spectroscopy of normal human brain and brain tumors*. Radiology, 1990. 174(2): p. 401-9.
2. Maintz, D., et al., *Phosphorus-31 MR spectroscopy of normal adult human brain and brain tumours*. NMR Biomed, 2002. 15(1): p. 18-27.
3. Alger, J.R., et al., *Metabolism of human gliomas: assessment with H-1 MR spectroscopy and F-18 fluorodeoxyglucose PET*. Radiology, 1990. 177(3): p. 633-41.
4. Obruchkov, S., *Echo Planar Spectroscopic Imaging and 31P In Vivo Spectroscopy*. , in *Open Access Distertations and Theses. Paper 4121.*,2011, McMaster University.
5. Srinivasa-Raghavan, R., et al. *31P Spectroscopic Imaging with GRAPPA*. in *Conference Proceedings of 17th International Society of Magnetic Resonance in Medicine*. 2009. Hawaii, USA.
6. Lustig, M., D. Donoho, and J.M. Pauly, *Sparse MRI: The application of compressed sensing for rapid MR imaging*. Magn Reson Med, 2007. 58(6): p. 1182-95.
7. Hu, S., et al., *Compressed sensing for resolution enhancement of hyperpolarized 13C flyback 3D-MRSI*. J Magn Reson, 2008. 192(2): p. 258-64.
8. Hu, S., et al., *3D compressed sensing for highly accelerated hyperpolarized (13)C MRSI with in vivo applications to transgenic mouse models of cancer*. Magn Reson Med, 2010. 63(2): p. 312-21.
9. Poole, M., *Improved Equipment and Techniques for Dynamic Shimming in High Field MRI*, in *Public ITEE2007*, The University of Queensland Australia.
10. Bloch, F., *The Principle of Nuclear Induction*. Science, 1953. 118(3068): p. 425-30.
11. Purcell E, T.H., Pound R, *Resonance absorption by nuclear magnetic moments in a solid*. Phys Rev, 1946. 69: p. 37-38.
12. E, S., *Quantisierung als Eigenwertproblem; von Erwin Schrodinger* Annalen der Psysik, 1926: p. 361-377.

13. Nelson, S.J., *Multivoxel magnetic resonance spectroscopy of brain tumors*. Mol Cancer Ther, 2003. 2(5): p. 497-507.
14. Star-Lack, J., et al., *Improved water and lipid suppression for 3D PRESS CSI using RF band selective inversion with gradient dephasing (BASING)*. Magn Reson Med, 1997. 38(2): p. 311-21.
15. Tran, T.K., et al., *Very selective suppression pulses for clinical MRSI studies of brain and prostate cancer*. Magn Reson Med, 2000. 43(1): p. 23-33.
16. Ozturk-Isik, E., et al., *Unaliasing lipid contamination for MR spectroscopic imaging of gliomas at 3T using sensitivity encoding (SENSE)*. Magn Reson Med, 2006. 55(5): p. 1164-9.
17. Hu, S., et al., *In vivo carbon-13 dynamic MRS and MRSI of normal and fasted rat liver with hyperpolarized 13C-pyruvate*. Mol Imaging Biol, 2009. 11(6): p. 399-407.
18. Salibi N., B.M.A., *Clinical MR Spectroscopy First Principles*. 1998: Wiley-Liss, Inc.
19. Ordidge, R., A. Connelly, and J.A. Lohman, , *Image-selected in vivo spectroscopy (ISIS): A new technique for spatially selective NMR spectroscopy*. J Magn Reson Imaging, 1986. 66: p. 283-294.
20. Chui, C.K., *An Introduction to Wavelets*. 1992, San Diego: Academic Press. ISBN 0-12-174584-8.
21. Candes, E.J.a.J.R., *Practical signal recovery from random projections*. in Proc. SPIE Computational Imaging, 2005.
22. Bertero M, B.P., *Introduction to Inverse Problems in Imaging*. . 1998, Bristol and Philadelphia: IOP Publishing Ltd.
23. Sarkar T, W.D., Jain V., *Some mathematical considerations in dealing with the inverse problem*. . IEEE Trans Antennas and Propagation, 1981. AP-29(2):373-379.
24. Hestenes M., S.E., *Methods of Conjugate Gradients for Linear Systems*. Journal of Research of the National Bureau of Standards, 1952. 49(6):2379.
25. Shewchuk, J., *An introduction to the conjugate gradient method without the agonizing pain*. 1994.
26. S, G., *Primer of Biostatistics*. 2001: McGraw Hill. 282-287 and 354-360.

27. Vanhamme, L., et al., *Time-domain quantification of series of biomedical magnetic resonance spectroscopy signals*. J Magn Reson, 1999. 140(1): p. 120-30.

APPENDIX A

Algorithm A.1. MATLAB Create Simulated Signal

```

function data = create_simulated_signal
tn=0.000333*[0:1023];

%Simulated 50 ms 500 ms 3200 ms 4000 ms
fk=[0 -124 -387 -826 152 179 248 321 349];
dk=[30 30 30 30 30 30 30 30 30];
ak=[1.990 1.263 1.237 0.581 0.8609 1.166 0.6315 0.9384 0.6136];
ph=[0 0 0 0];
yn=0;
%Simulated 50 ms 500 ms 3200 ms 4000 ms
fk_t=[0 -124 -387 -826 152 179 248 321 349];
dk_t=[30 30 30 30 30 30 30 30 30];
ak_t=[0.990 1.263 1.237 0.581 1.8609 2.166 0.9315 1.9384 1.6136];
ph_t=[0 0 0 0];
yn_t=0;
for n=1:size(ak,1)
    for m=1: size(ak,2)
        yn=yn+(ak(n,m)*exp(i*ph(n)*180/pi)*exp((-dk(n,m)+i*2*pi*fk(n,m))*tn));
    end
end
for n=1:size(ak_t,1)
    for m=1: size(ak_t,2)
        yn_t=yn_t+(ak_t (n,m)*exp(i*ph_t(n)*180/pi)*exp((-
dk_t(n,m)+i*2*pi*fk_t(n,m))*tn));
    end
end
yn_f=fftshift(fft(yn));
yn_tf=fftshift(fft(yn_t));
noise_1 = rand([1,1024])*max(abs(yn_f(:)))*0.08;
yn_f = yn_f+noise_1;
noise_2 = rand([1,1024])*max(abs(yn_tf(:)))*0.08;
yn_tf = yn_tf+noise_2;
data=zeros(32,32,1024);
for m=1:32
    for n=1:32
        if (m<=10 & n<=10)
            data(m,n,:)=yn_tf;
        elseif m>10
            data(m,n,:)=yn_f;
        elseif m<=10 & n>10
            data(m,n,:)=yn_f;
        end
    end
end
end

```

APPENDIX B

Algorithm B.1. MATLAB P31 MRSI Simulation

```

clear all;
close all;
addpath(strcat(pwd, '/utils'));
addpath(strcat(pwd, '/wavelab850'));
wavePath;

p31= create_simulated_signal;
% imshow(squeeze(real(p31(:,:,381))))
p31_f = fftshift(fft(p31));
figure; imshow(squeeze(abs(p31_f(:,:,513))), [0 max(abs(p31_f(:)))]);
p31_rec= ifftn(ifftshift(p31_f));
figure; imshow(squeeze(abs(p31_rec(:,:,513))), [0 max(abs(p31_rec(:)))]);
figure; plot(squeeze(real(p31_rec(4,4,:))));

%Select lines for zeros and create arrays with some random
%undersampling
mask_all = ones(32,32,1024);
p31_fu=p31_f;
k_center=2;
k_down=32/2-k_center/2;
k_up=32/2+k_center/2;
ind=round(rand(15,1)*k_down);
indz=find(ind==0);
ind(indz)=1;
mask_all(ind,,:)=0;
mask_all(k_up+ind,,:)=0;
maskz=find(mask_all==0);
p31_fu(maskz)= 0;
p31_fu_rec= ifftn(ifftshift(p31_fu));

figure; imshow(squeeze(abs(p31_fu_rec(:,:,513))), [0 max(abs(p31_fu_rec(:)))]);
figure; plot(squeeze(real(p31_fu_rec(4,15,:))));

p31_fu_hrec = ifft(fftshift(p31_fu,2), [],2);

figure; plot(squeeze(real(p31_fu_hrec(:,1,:))));

for n=1:32
    %Select lines for zeros and create arrays with some random
    %undersampling
    im_z= squeeze(p31_fu_hrec(:,n,:));
    mask = squeeze(mask_all(:,n,:));
    data= im_z;
    imshow(abs(data));
    pdf = mask;

```

```

%%%%%%%%%%%%%%%%%%%%%%%%%%%%%%%%%%%%%%%%%%%%%%%%%%%%%%%%%%%%%%%%%%%%%%%%
% L1 Recon Parameters
%%%%%%%%%%%%%%%%%%%%%%%%%%%%%%%%%%%%%%%%%%%%%%%%%%%%%%%%%%%%%%%%%%%%%%%%

N = size(data);      % image Size
DN = size(data);    % data Size
TVweight = 0.01;    % weight for TV penalty
xfmweight = 0.01;   % weight for Transform L1 penalty
Itnlm = 15;         % Number of iterations

    phmask = zpad(hamming(6)*hamming(6)',N(1),N(2)); %mask to grab center
frequency
    phmask = phmask/max(phmask(:));                %for low-order phase
estimation and correction
    ph = exp(i*angle((ifft2c(data.*phmask)))); % estimate phase for phase
correction

%generate Fourier sampling operator
FT = p2DFT(mask, N, ph, 2);

% scale data
im_dc = FT'*(data);%.*mask);%./pdf);
data = data/max(abs(im_dc(:)));
im_dc = im_dc/max(abs(im_dc(:)));

%generate transform operator
%XFM = wavelet('Daubechies',6,4); % wavelet
%XFM = 1;
XFM = wavelet('Daubechies',4,4); % wavelet

% initialize Parameters for reconstruction

param = init;
param.FT = FT;
param.XFM = XFM;
param.TV = TVOP;
param.data = data;
param.TVweight =TVweight;      % TV penalty
param.xfmweight = xfmweight;    % L1 wavelet penalty
param.Itnlm = Itnlm;
%   figure(100), imshow(abs(im_dc),[]);drawnow;
res = XFM*im_dc;
% figure; imshow(abs(res))
% do iterations
tic
for iter=1:5
    res = fnlCg(res,param);
    im_res = XFM'*res;
end
toc

p31_res(:,n,:)=fftshift(im_res);
end

```

```
figure; imshow(squeeze(abs(p31_res(:,:,513))), [0 max(abs(p31_res(:))]);  
figure; plot(squeeze(real(p31_res(4,4,:))));  
  
m=20;n=1;  
  
figure; subplot(3,1,1);plot(squeeze(real(p31(m,n,:)))  
hold on; subplot(3,1,2);plot(squeeze(real(p31_fu_rec(m,n,:)))  
hold on; subplot(3,1,3);plot(squeeze(real(p31_res(m,n,:)))
```

APPENDIX C

Algorithm C.1. MATLAB Bland Altman Test

```

% Calculates the Bland Altman statistics given two datasets named orig and
% newm.
% bland_altman_stat is 0 if the difference between the two datasets has any
% points lying outside the 2*sd(difference) from the mean of the
% difference. It is 1 if all the difference data resides within 2*SD.
% outlcount is the number of outlier points if there are any.
% meandiff is the mean of the difference between the two datasets.
% stddiff is the std of the difference between the two datasets.

% Esin Ozturk, UCSF

function [bland_altman_stat, outlcount,meandiff,stddiff] = bland_altman(orig,
newm)
diffm = abs(orig-newm);
avgm = abs(orig+newm)./2;
stddiff = std(diffm);
meandiff = mean(diffm);

outlcount = length(find(diffm>meandiff+2*stddiff))+length(find(diffm<meandiff-
2*stddiff));
bland_altman_stat = isequal(outlcount,0);
size(avgm);
x1 = [0, max(avgm)];
y1 = [meandiff, meandiff];
x2 = [0, max(avgm)];
y2 = [meandiff+2*stddiff, meandiff+2*stddiff];
x3 = [0, max(avgm)];
y3 = [meandiff-2*stddiff, meandiff-2*stddiff];
figure;
plot(avgm, diffm, '.'); hold on; line(x1,y1); hold on; line(x2,y2); hold on;
line(x3,y3)

```

APPENDIX D

Algorithm D.1. MATLAB Calculate Estimates

```

% PCr gATP aATP bATP GPC GPE Pi PC PE noise
ranges = [{510:516}, {460:480}, {370:390}, {220:240}, {560:570}, {570:585},
{590:610}, {610:625}, {625:640}, {850:900}];
for n=1:9
    Orig(n,:,:)= max(squeeze(real(p31(:,:,ranges{n}))), [], 3);
end

Orig(10,:,:)= std(squeeze(real(p31(:,:,ranges{10}))), 0, 3);

for n=1:9
    CS(n,:,:)= max(squeeze(real(p31_res(:,:,ranges{n}))), [], 3);
end

CS(10,:,:)= std(squeeze(real(p31_res(:,:,ranges{10}))), 0, 3);

Pi_PCr_o = squeeze(Orig(7,:,:)./Orig(1,:,:));
Pi_PCr_cs = squeeze(CS(7,:,:)./CS(1,:,:));
PCr_bATP_o=squeeze(Orig(1,:,:)./Orig(4,:,:));
PCr_bATP_cs=squeeze(CS(1,:,:)./CS(4,:,:));
PCr_PE_o=squeeze(Orig(1,:,:)./Orig(9,:,:));
PCr_PE_cs=squeeze(CS(1,:,:)./CS(9,:,:));

SNR_PCr_o= squeeze(Orig(1,:,:)./Orig(10,:,:));
SNR_PCr_cs= squeeze(CS(1,:,:)./CS(10,:,:));
SNR_Pi_o= squeeze(Orig(7,:,:)./Orig(10,:,:));
SNR_Pi_cs= squeeze(CS(7,:,:)./CS(10,:,:));
SNR_bATP_o= squeeze(Orig(4,:,:)./Orig(10,:,:));
SNR_bATP_cs= squeeze(CS(4,:,:)./CS(10,:,:));

ph_PCr_o= squeeze(Orig(1,:,:));
ph_PCr_cs= squeeze(CS(1,:,:));
ph_Pi_o= squeeze(Orig(7,:,:));
ph_Pi_cs= squeeze(CS(7,:,:));
ph_bATP_o= squeeze(Orig(4,:,:));
ph_bATP_cs= squeeze(CS(4,:,:));

Pi_PCr_o_t = Pi_PCr_o(1:10,1:10);
Pi_PCr_o_h= Pi_PCr_o(11:32,11:32);
Pi_PCr_cs_t = Pi_PCr_cs(1:10,1:10);
Pi_PCr_cs_h = Pi_PCr_cs(11:32,11:32);

PCr_bATP_o_t = PCr_bATP_o(1:10,1:10);
PCr_bATP_o_h= PCr_bATP_o(11:32,11:32);

```

```

PCr_bATP_cs_t = PCr_bATP_cs(1:10,1:10);
PCr_bATP_cs_h = PCr_bATP_cs(11:32,11:32);

PCr_PE_o_t = PCr_PE_o(1:10,1:10);
PCr_PE_o_h= PCr_PE_o(11:32,11:32);
PCr_PE_cs_t = PCr_PE_cs(1:10,1:10);
PCr_PE_cs_h = PCr_PE_cs(11:32,11:32);

SNR_PCr_o_t = SNR_PCr_o(1:10,1:10);
SNR_PCr_o_h= SNR_PCr_o(11:32,11:32);
SNR_PCr_cs_t = SNR_PCr_cs(1:10,1:10);
SNR_PCr_cs_h = SNR_PCr_cs(11:32,11:32);

SNR_Pi_o_t = SNR_Pi_o(1:10,1:10);
SNR_Pi_o_h= SNR_Pi_o(11:32,11:32);
SNR_Pi_cs_t = SNR_Pi_cs(1:10,1:10);
SNR_Pi_cs_h = SNR_Pi_cs(11:32,11:32);

SNR_bATP_o_t = SNR_bATP_o(1:10,1:10);
SNR_bATP_o_h= SNR_bATP_o(11:32,11:32);
SNR_bATP_cs_t = SNR_bATP_cs(1:10,1:10);
SNR_bATP_cs_h = SNR_bATP_cs(11:32,11:32);

ph_PCr_o_t = ph_PCr_o(1:10,1:10);
ph_PCr_o_h= ph_PCr_o(11:32,11:32);
ph_PCr_cs_t = ph_PCr_cs(1:10,1:10);
ph_PCr_cs_h = ph_PCr_cs(11:32,11:32);

ph_Pi_o_t = ph_Pi_o(1:10,1:10);
ph_Pi_o_h= ph_Pi_o(11:32,11:32);
ph_Pi_cs_t = ph_Pi_cs(1:10,1:10);
ph_Pi_cs_h = ph_Pi_cs(11:32,11:32);

ph_bATP_o_t = ph_bATP_o(1:10,1:10);
ph_bATP_o_h= ph_bATP_o(11:32,11:32);
ph_bATP_cs_t = ph_bATP_cs(1:10,1:10);
ph_bATP_cs_h = ph_bATP_cs(11:32,11:32);

fprintf('mean+-std Pi/PCr original tumor = %f+-%f\n', mean(Pi_PCr_o_t(:)),
std(Pi_PCr_o_t(:)));
fprintf('mean+-std Pi/PCr cs tumor = %f+-%f\n', mean(Pi_PCr_cs_t(:)),
std(Pi_PCr_cs_t(:)));
fprintf('mean+-std Pi/PCr original healthy = %f+-%f\n', mean(Pi_PCr_o_h(:)),
std(Pi_PCr_o_h(:)));
fprintf('mean+-std Pi/PCr cs healthy = %f+-%f\n', mean(Pi_PCr_cs_h(:)),
std(Pi_PCr_cs_h(:)));

clc
fprintf('mean+-std PCr/b-ATP original tumor = %f+-%f\n', mean(PCr_bATP_o_t(:)),
std(PCr_bATP_o_t(:)));
fprintf('mean+-std PCr/b-ATP cs tumor = %f+-%f\n', mean(PCr_bATP_cs_t(:)),
std(PCr_bATP_cs_t(:)));
fprintf('mean+-std PCr/b-ATP original healthy = %f+-%f\n',
mean(PCr_bATP_o_h(:)), std(PCr_bATP_o_h(:)));
fprintf('mean+-std PCr/b-ATP cs healthy = %f+-%f\n', mean(PCr_bATP_cs_h(:)),

```

```

std(PCr_bATP_cs_h(:)));

clc
fprintf('mean+-std PCr/PE original tumor = %f+-%f\n', mean(PCr_PE_o_t(:)),
std(PCr_PE_o_t(:)));
fprintf('mean+-std PCr/PE cs tumor = %f+-%f\n', mean(PCr_PE_cs_t(:)),
std(PCr_PE_cs_t(:)));
fprintf('mean+-std PCr/PE original healthy = %f+-%f\n', mean(PCr_PE_o_h(:)),
std(PCr_PE_o_h(:)));
fprintf('mean+-std PCr/PE cs healthy = %f+-%f\n', mean(PCr_PE_cs_h(:)),
std(PCr_PE_cs_h(:)));

clc
fprintf('mean+-std SNR PCr original tumor = %f+-%f\n', mean(SNR_PCr_o_t(:)),
std(SNR_PCr_o_t(:)));
fprintf('mean+-std SNR PCr cs tumor = %f+-%f\n', mean(SNR_PCr_cs_t(:)),
std(SNR_PCr_cs_t(:)));
fprintf('mean+-std SNR PCr original healthy = %f+-%f\n', mean(SNR_PCr_o_h(:)),
std(SNR_PCr_o_h(:)));
fprintf('mean+-std SNR PCr cs healthy = %f+-%f\n', mean(SNR_PCr_cs_h(:)),
std(SNR_PCr_cs_h(:)));

clc
fprintf('mean+-std SNR Pi original tumor = %f+-%f\n', mean(SNR_Pi_o_t(:)),
std(SNR_Pi_o_t(:)));
fprintf('mean+-std SNR Pi cs tumor = %f+-%f\n', mean(SNR_Pi_cs_t(:)),
std(SNR_Pi_cs_t(:)));
fprintf('mean+-std SNR Pi original healthy = %f+-%f\n', mean(SNR_Pi_o_h(:)),
std(SNR_Pi_o_h(:)));
fprintf('mean+-std SNR Pi cs healthy = %f+-%f\n', mean(SNR_Pi_cs_h(:)),
std(SNR_Pi_cs_h(:)));

clc
fprintf('mean+-std SNR bATP original tumor = %f+-%f\n', mean(SNR_bATP_o_t(:)),
std(SNR_bATP_o_t(:)));
fprintf('mean+-std SNR bATP cs tumor = %f+-%f\n', mean(SNR_bATP_cs_t(:)),
std(SNR_bATP_cs_t(:)));
fprintf('mean+-std SNR bATP original healthy = %f+-%f\n',
mean(SNR_bATP_o_h(:)), std(SNR_bATP_o_h(:)));
fprintf('mean+-std SNR bATP cs healthy = %f+-%f\n', mean(SNR_bATP_cs_h(:)),
std(SNR_bATP_cs_h(:)));

clc
fprintf('Ratio of mean SNR PCr original tumor/healthy = %f\n',
mean(SNR_PCr_o_t(:))/ mean(SNR_PCr_o_h(:)));
fprintf('Ratio of mean SNR PCr cs tumor/healthy = %f\n', mean(SNR_PCr_cs_t(:))/
mean(SNR_PCr_cs_h(:)));
fprintf('Ratio of mean SNR Pi original tumor/healthy = %f\n',
mean(SNR_Pi_o_t(:))/ mean(SNR_Pi_o_h(:)));
fprintf('Ratio of mean SNR Pi cs tumor/healthy = %f\n', mean(SNR_Pi_cs_t(:))/
mean(SNR_Pi_cs_h(:)));
fprintf('Ratio of mean SNR bATP original tumor/healthy = %f\n',
mean(SNR_bATP_o_t(:))/ mean(SNR_bATP_o_h(:)));

```



```

fprintf('Ratio of mean SNR bATP cs tumor/healthy = %f\n',
mean(SNR_bATP_cs_t(:))/ mean(SNR_bATP_cs_h(:)));

clc

fprintf('Ratio of mean ph PCr original tumor/healthy = %f\n',
mean(ph_PCr_o_t(:))/ mean(ph_PCr_o_h(:)));
fprintf('Ratio of mean ph PCr cs tumor/healthy = %f\n', mean(ph_PCr_cs_t(:))/
mean(ph_PCr_cs_h(:)));
fprintf('Ratio of mean ph Pi original tumor/healthy = %f\n',
mean(ph_Pi_o_t(:))/ mean(ph_Pi_o_h(:)));
fprintf('Ratio of mean ph Pi cs tumor/healthy = %f\n', mean(ph_Pi_cs_t(:))/
mean(ph_Pi_cs_h(:)));
fprintf('Ratio of mean ph bATP original tumor/healthy = %f\n',
mean(ph_bATP_o_t(:))/ mean(ph_bATP_o_h(:)));
fprintf('Ratio of mean ph bATP cs tumor/healthy = %f\n', mean(ph_bATP_cs_t(:))/
mean(ph_bATP_cs_h(:)));

[BAS_Pi_PCr_t, outl_Pi_PCr_t,mdiff_Pi_PCr_t,sdiff_Pi_PCr_t] =
bland_altman(Pi_PCr_o_t(:), Pi_PCr_cs_t(:))
[BAS_Pi_PCr_h, outl_Pi_PCr_h,mdiff_Pi_PCr_h,sdiff_Pi_PCr_h] =
bland_altman(Pi_PCr_o_h(:), Pi_PCr_cs_h(:))
[BAS_PCr_bATP_t, outl_PCr_bATP_t,mdiff_PCr_bATP_t,sdiff_PCr_bATP_t] =
bland_altman(PCr_bATP_o_t(:), PCr_bATP_cs_t(:))
[BAS_PCr_bATP_h, outl_PCr_bATP_h,mdiff_PCr_bATP_h,sdiff_PCr_bATP_h] =
bland_altman(PCr_bATP_o_h(:), PCr_bATP_cs_h(:))
[BAS_PCr_PE_t, outl_PCr_PE_t,mdiff_PCr_PE_t,sdiff_PCr_PE_t] =
bland_altman(PCr_PE_o_t(:), PCr_PE_cs_t(:))
[BAS_PCr_PE_h, outl_PCr_PE_h,mdiff_PCr_PE_h,sdiff_PCr_PE_h] =
bland_altman(PCr_PE_o_h(:), PCr_PE_cs_h(:))

[p_SNR_PCr_o,h_SNR_PCr_o]=ranksum(SNR_PCr_o_t(:), SNR_PCr_o_h(:))
[p_SNR_PCr_cs,h_SNR_PCr_cs]=ranksum(SNR_PCr_cs_t(:), SNR_PCr_cs_h(:))
[p_SNR_Pi_o,h_SNR_Pi_o]=ranksum(SNR_Pi_o_t(:), SNR_Pi_o_h(:))
[p_SNR_Pi_cs,h_SNR_Pi_cs]=ranksum(SNR_Pi_cs_t(:), SNR_Pi_cs_h(:))
[p_SNR_bATP_o,h_SNR_bATP_o]=ranksum(SNR_bATP_o_t(:), SNR_bATP_o_h(:))
[p_SNR_bATP_cs,h_SNR_bATP_cs]=ranksum(SNR_bATP_cs_t(:), SNR_bATP_cs_h(:))

```